NISTIR 89-4079

DETERMINATION OF FIBER/MATRIX INTERFACIAL PROPERTIES OF CERAMIC AND GLASS MATRIX COMPOSITES

David C. Cranmer

U.S. DEPARTMENT OF COMMERCE
National Institute of Standards
and Technology
Ceramics Division
Gaithersburg, MD 20899

This program supported in part by the
Strategic Defense Initiative Office/
Innovative Science and Technology
under ONR Contract
Contract Number - N00014-86-F-0096

U.S. DEPARTMENT OF COMMERCE
Robert A. Mosbacher, Secretary

Lee Mercer, Deputy Under Secretary
for Technology

NATIONAL INSTITUTE OF STANDARDS
AND TECHNOLOGY
Raymond G. Kammer, Acting Director

NIST

NISTIR 89-4079

DETERMINATION OF FIBER/MATRIX INTERFACIAL PROPERTIES OF CERAMIC AND GLASS MATRIX COMPOSITES

David C. Cranmer

U.S. DEPARTMENT OF COMMERCE
National Institute of Standards and Technology
Ceramics Division
Gaithersburg, MD 20899

This program supported in part by the Strategic Defense Initiative Office/ Innovative Science and Technology under ONR Contract
Contract Number - N00014-86-F-0096

February 1990

U.S. DEPARTMENT OF COMMERCE
Robert A. Mosbacher, Secretary
Lee Mercer, Deputy Under Secretary for Technology
NATIONAL INSTITUTE OF STANDARDS AND TECHNOLOGY
Raymond G. Kammer, Acting Director

Determination of Fiber/Matrix Interfacial Properties of Ceramic and Glass Matrix Composites

Table of Contents

FORWARD

This report summarizes work performed from 1986 to 1988 at the National Institute of Standards and Technology on the measurement and characterization of fiber/matrix interfaces in a variety of ceramic and glass matrix composites. A number of people have contributed to the work presented in this report including Steve Freiman, Ed Fuller, Tom Coyle, Uday Deshmukh, Tom Palamides, Mike Barsoum, and Mike Koczak. Funding for the work described has been provided by a number of sources including the Stategic Defense Initiative Office/Innovative Science and Technology under ONR contract N00014-C-0096, the Department of Energy Fossil Energy Materials Program, and NIST.

The work described herein is primarily related to the development and use of several techniques for determining the fiber/matrix interfacial properties of ceramic and glass matrix composites. The specific techniques utilized are the double cleavage drilled compression (DCDC), indentation push-in, indentation push-out, and single fiber pull-out tests. The DCDC test provides direct experimental observation of the crack-fiber interactions, thus allowing us to more readily determine the effects of the fiber/matrix interface on the properties of the composites. The indentation techniques and the pull-out test provide information on the debond strength of the fibers from the matrix and interfacial frictional stress required to pull the fibers out of the matrix.

The emphasis has been on understanding what happens at the interface, and has focussed on several model systems including SiC monofilament reinforced glasses (borosilicate, soda-lime-silica),and SiC fiber reinforced glass-ceramic. Measurements have been made of the interface properties as well as on the increase in toughness as a crack approaches the reinforcing fibers. Some of the effects of interface chemistry on the properties have also been considered, both experimentally and as it might relate to processing of the composite. Much of the work is expected to continue with a future emphasis on the high temperature aspects of ceramic and glass matrix composites.

Ceram. Eng. Sci. Proc., 8 [7-8] pp. 630-635 (1987)

Fracture Mechanics Characterization of Crack/Fiber Interactions in Ceramic Matrix Composites

T. W. COYLE, E. R. FULLER, JR., AND P. SWANSON

Ceramics Div., Inst. Materials Sci. and Eng.
National Bureau of Standards, Gaithersburg, MD 20899

T. PALAMIDES

Drexel Univ.
Philadelphia, PA

A crucial factor in the structural performance of ceramic matrix composites is the influence of the fiber/matrix bond on the interaction of a matrix crack with the reinforcing fibers. To elucidate the character of this interaction under controlled fracture conditions, glass fracture mechanics specimens were fabricated in the double-cleavage, drilled compression (DCDC) configuration with simple arrays of fibers. Propagating cracks were observed in cross-polarized illumination to characterize delamination of the fiber ahead of the crack and bridging interactions behind the crack tip. Stress wave fractography was employed to analyze the shape and relative velocity of the crack front.

Introduction

A critical issue in the fracture behavior and mechanical performance of ceramic matrix composites is the influence of the strength of the fiber/matrix interface on the interaction of a crack with individual fibers. It is generally accepted that if a strong bond is present between fiber and matrix, cracks run directly through the reinforcing fibers which then have little effect on retarding the propagation of the crack. Although the strength of such a composite may be enhanced through load transfer, the toughness is not appreciably improved and failure is completely brittle. A weak interface leads to crack deflection, debonding along the fiber/matrix interface, and bridging of the crack by the fibers. If the fibers do not break behind the crack tip failure is non-catastrophic. However, if the interface is too weak the fibers slide freely through the matrix and no improvement in strength or toughness is obtained. Thus, a better understanding of the details of this behavior is required before the optimum levels of interfacial strength can be determined for a given fiber-matrix system.

This issue can be investigated experimentally by direct observation of the interaction of a crack with a single fiber in an appropriate fracture mechanics specimen. The double cleavage drilled compression (DCDC) configuration[1] was employed because of the simple shape and loading geometry. No guiding side grooves are required to keep the plane of the crack in the center of this compressively loaded specimen.

Stable crack propagation is obtained in the DCDC specimen since the applied stress intensity (K_{app}) experienced at the crack tip decreases with crack extension at a constant load. From the measured crack length (c) at a given remotely applied compressive stress (σ_{app}), K_{app} can be calculated from the following expression:[1]

$$K_{app} = \sigma_{app}\sqrt{r}\,/[(c/r)f(c/r)] \qquad (1)$$

where the specimen dimensions are as defined in Fig. 1. The function $f(c/r)$ can be determined experimentally by testing specimens of known K_{IC}.

Experimental Procedure

. Transparent specimens were produced by sandwiching SiC fibers* between borosilicate glass plates† which were then fused together by heating in air at approximately 850 °C for 10–15 min to produce transparent specimens. The samples were loaded in compression with a screw-driven mechanical testing machine‡ at a crosshead displacement rate of 0.005 cm/min. The strain contours visible in cross-polarized illumination were used to monitor the length of the growing crack and to characterize the crack-fiber interactions.

Stress wave fractography[2] was utilized to monitor the shape of the crack front and the relative velocity of the growing crack along the specimen. Acoustic waves were propagated through the specimen during crack extension by use of a piezoceramic transducer coupled to the specimen. The transducer was driven with bursts of an 80–90 kHz sine wave at a maximum of 30 V peak-to-peak. The burst frequency was 5 Hz; the burst duration was 25% of the low frequency period. This technique produce ripples on the fracture surface at a spacing determined by the frequency of the acoustic excitation. These ripples can then be observed by optical microscopy in reflected light using Nomarsky contrast. With a constant excitation frequency, widely spaced bands indicate a region of rapid crack extension while closely spaced bands indicate relatively slow crack growth.

Results and Discussion

Direct, qualitative observations of several aspects of the fracture behavior in the specimen could be made in transmitted, cross-polarized illumination at various magnifications. Typically the fiber could be seen to bridge the crack for some distance behind the crack tip before breaking. Evidence of localized strain at the fiber-crack surface intersection (Fig. 2) indicated that the bridging fiber was applying tractions across the crack faces. The shape of the strain contours ahead of the crack tip or behind the crack tip away from the crack surfaces gave only occasional faint indications of localized strain which would show load transfer to the fiber. Apparent delamination of the fiber ahead of the crack (Fig. 3) was observed when a higher magnification was used for one specimen.

An optical micrograph of a region of the fracture surface which includes a fiber, taken with Nomarsky contrast, is shown in Fig. 4. The light and dark bands visible under these conditions represent snapshots of the position and shape of the crack front at periodic intervals. It can be seen that the crack front bowed around the fiber which was bridging the crack before the center portion broke away and accelerated to reform a nearly straight front. A scanning electron micrograph of this area (Fig. 5) shows that after bowing around the fiber the two sides of the crack did not meet on the same plane. The resulting ligament would have to have fractured before the center portion of the crack front could extend. From the direct observations discussed above, the fiber appears to have broken at some later time, after the ligament had fractured and the crack front had moved well beyond the fiber. The chipping apparent around the fiber in Fig. 5 would have occurred as the broken fiber was pulled out of the glass matrix.

*SCS-6 Fibers, Avco Corp., Wilmington, MA.
†Corning 7740, Corning Glass Works, Corning, NY.
‡Instron Corp., Canton, MA.

To quantitatively assess the influence of the fibers on the crack propagation the crack length was measured from photographs, such as shown in Fig. 2, and used to calculate the apparent K_{app} from the applied load using Eq. (1). The results for several specimens are shown in Fig. 6. Assuming that the crack is growing at a constant stress intensity, $K_{tip}=K_{IC}$ for the glass matrix, the increase in the calculated K_{app} for crack lengths beyond the fiber position reflects the closure tractions exerted by the bridging fiber (K_{trac}).

$$K_{tip}=K_{IC}=K_{app}=K_{trac} \tag{2}$$

or

$$K_{trac}=K_{IC}-K_{app} \tag{3}$$

The stress intensity factor due to a point force acting at a distance δ behind the crack tip is given by:[3]

$$K_{trac}=-\sqrt{2}\,F/(\pi\delta)^{3/2} \tag{4}$$

where the point force, F, may be a function of δ. Thus, information regarding the forces exerted by the bridging fiber as a function of crack length can be obtained from data such as shown in Fig. 6.

Summary

Sample fabrication methods and experimental techniques have been developed which allow crack-fiber interactions to be directly examined in a ceramic matrix. Qualitative information regarding fiber/matrix debonding, fiber bridging, and pinning and bowing of the crack front at the fiber can be obtained. Possibilities for quantifying the effects of bridging fibers on crack extension in terms of the tractions exerted across the crack by the fiber were demonstrated.

Acknowledgments

Support for this work has been provided by the Department of Energy AR&TD Fossil Energy Materials Program (DE-AI05-800R20679) and by the SDIO/IST program under ONR contract No. N00014-86-F-0096.

References

[1]C. Janssen, "Specimen for Fracture Mechanics Studies on Glass;" pp. 23-30 in Proceedings of the Xth International Congress on Glass, Kyoto, Japan, July 8-13, 1974. The Ceramic Society of Japan, Kyoto, Japan.

[2]H. Richter, "Crack Propagation in Glass Under Liquids in an Intermediate Range of Crack Velocities;" pp. 219-29 in Strength of Inorganic Glass, Ed. by C. R. Kurkjian, Plenum Publishing Corp., 1985.

[3]H. Tada, P. C. Paris, and G. R. Irwin, The Stress Analysis of Cracks Handbook, Del Research Corp., Hellertown, PA., 1973.

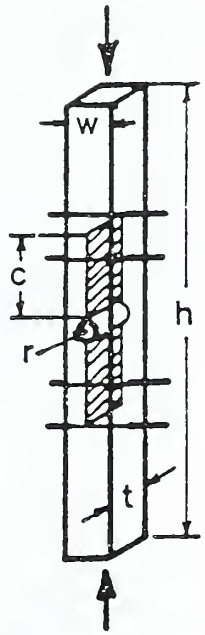

Fig. 1. Double-cleavage drilled-compression fracture mechanics specimen. Compressive load opens cracks above and below centered hole.

Fig. 2. View perpendicular to fiber axes of DCDC specimen under load. The cracks are seen edge-on with the crack tips located between the inner and outer fibers. Strain contours are visible by virtue of the transmitted cross-polarized illumination.

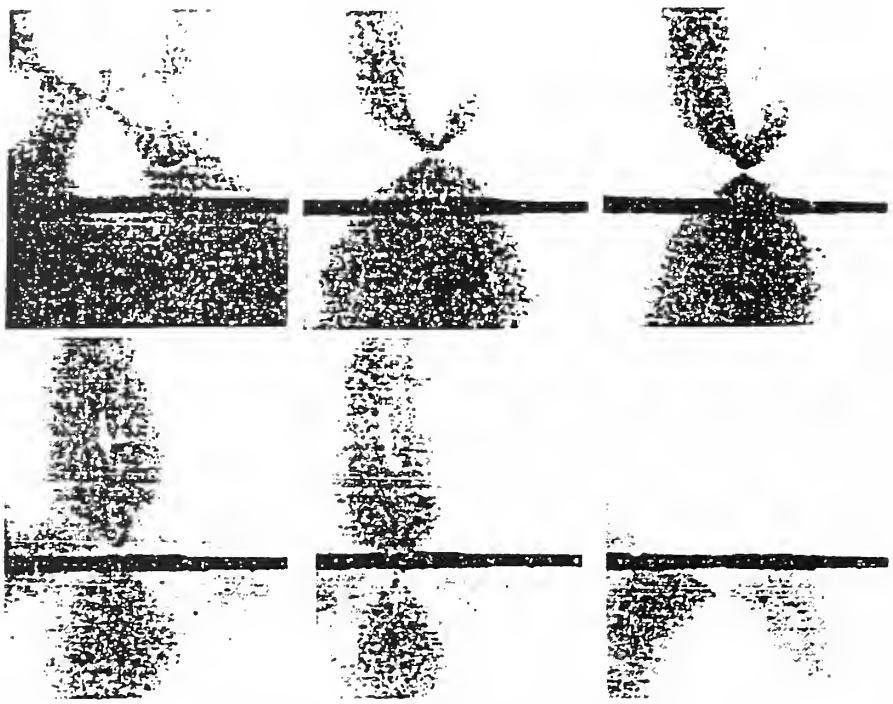

Fig. 3. Higher magnification views in cross-polarized transmitted light of region near reinforcing fiber. Crack-tip is seen approaching and then passing the fiber as the remotely applied load is increased. Field of view is approximately 2.7 mm wide.

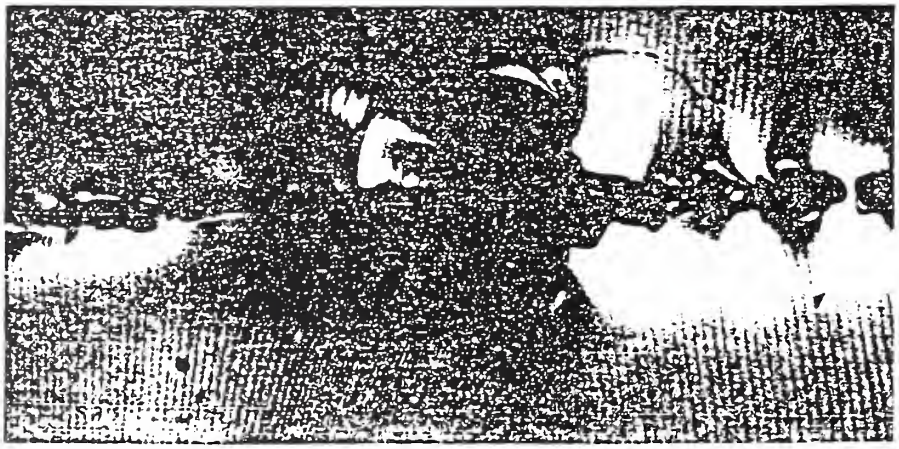

Fig. 4. Optical micrograph of a region of the fracture surface centered about a reinforcing fiber. Nomarsky contrast reveals the periodic surface undulations caused by the applied acoustic waves. The crack was propagating from right to left. The field of view is approximately 1 mm wide.

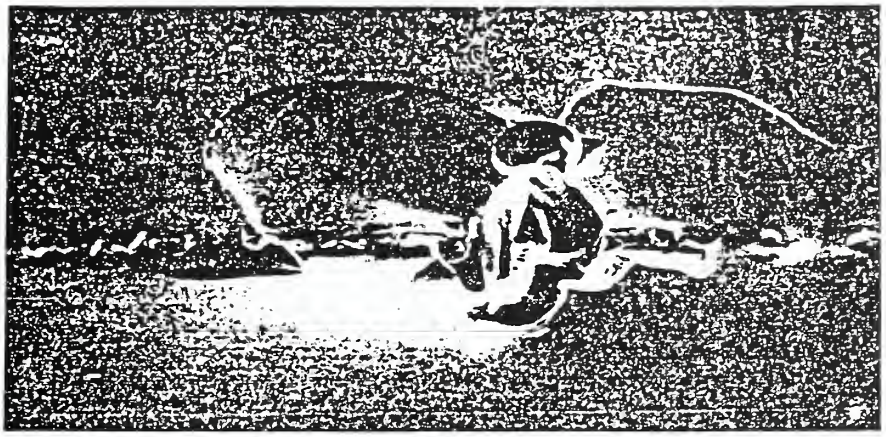

Fig. 5. Scanning electron micrograph of area shown in Fig. 4. The remnant of the ligament formed as the crack front swept around the fiber can be seen to the left of the fiber. (Field of view approximately 1.1 mm wide.)

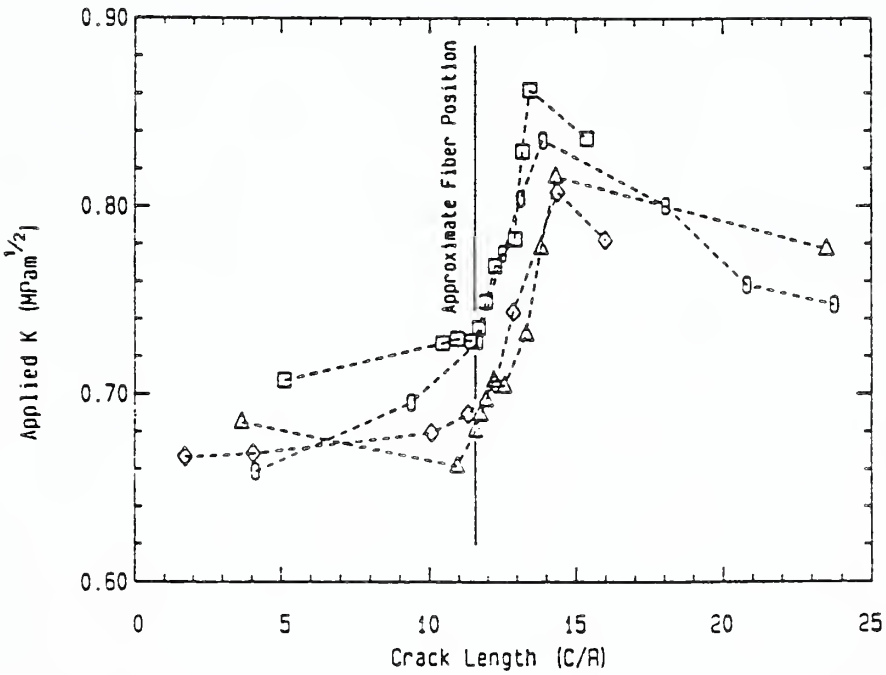

Fig. 6. Plot of remotely applied K (calculated from Eq. (1)) vs crack length showing relative position of the reinforcing fiber. Increase in the applied K required to propagate the crack reflects the closure forces exerted by the bridging fiber.

CRACK-FIBER INTERACTIONS IN CERAMIC MATRIX COMPOSITES

"To be published on Proceedings of 1987 Northeast Regional ASM Meeting"

T. W. Coyle, T. R. Palamides*, S. W. Freiman,
E. R. Fuller and U. V. Deshmukh*

Ceramics Division
Institute for Materials Science and Engineering
National Bureau of Standards
Gaithersburg, MD

*Drexel University
Philadelphia, PA

Abstract

Crack-fiber interactions are the key to the unique properties of continuous fiber reinforced ceramic matrix composites. This paper describes the development of a fracture mechanics technique for examining crack-fiber interactions in model SiC fiber reinforced glass specimens. Direct examination of the closure force imposed by a bridging fiber on a crack was accomplished using the double-cleavage drilled-compression sample. The stress intensity at the crack tip is described in terms of the applied load and the closure force. The closure force is a function of the interfacial bonding and/or frictional forces between the fiber and the matrix. Evaluation of these interfacial forces by indentation experiments in which the indentation load and the displacement of the fiber are measured directly is described.

Introduction

The fracture behavior of brittle matrix/brittle fiber composite systems is strongly dependent on the mechanical performance of the fiber/matrix interface. For a given set of fiber and matrix properties, the fracture characteristics can range from the desired fibrous, non-catastrophic failure to a completely brittle, low toughness fracture, depending on the interfacial properties. The first condition which must be met to avoid a completely brittle failure mode is for the interface to be weak enough to allow debonding to occur between the fiber and matrix ahead of the crack tip or to cause the matrix crack to deflect along the interface. Fracture mechanics treatments of cracks at bi-material interfaces[1,2] provide some guidance regarding the relative strength levels required among matrix, fiber, and interface to achieve the desired interfacial failure but direct experimental studies are lacking.

When the interface has debonded, the fiber can remain bridging between the crack faces after the matrix crack has advanced. Propagation of the matrix crack is then opposed by the closure forces exerted on the crack by the bridging fibers. The nature of these closure forces is controlled by the shear properties of the interface and the fiber modulus and strength. Recent modelling of this situation by Marshall, Evans and coworkers[3,4] indicates that the bridging fibers can either remain intact behind the crack tip leading to non-catastrophic failure or can break at some distance behind the crack tip resulting in a failure which is primarily brittle in nature, although with a higher toughness than the unreinforced matrix. Experimental results suggest that the trends predicted by the model with changes in interfacial character are correct, but detailed studies over the range of possible behavior are not yet available.

Direct experimental examination of the interactions between matrix cracks and reinforcing fibers is therefore valuable in furthering the understanding of the influence of interfacial properties on fracture behavior. Develop of techniques to investigate these issues are described in the following along with observations on a model ceramic matrix system, SiC fiber reinforced glass. The double cleavage drilled compression (DCDC) configuration[5] was used to study the effects of individual SiC fibers on crack propagation in glass specimens. Qualitative observations of the shape of the crack front and the fracture path in the vicinity of the fiber were made and some quantitative information regarding the closure forces exerted by bridging fiber was obtained. The fiber/matrix interfacial shear properties were evaluated independently by measuring the force required to push the fibers through thin sections of the glass matrix using an indentation technique. The results of these tests are discussed in terms of the current views of fracture in ceramic matrix composites.

Experimental Procedure

Transparent DCDC specimens were produced by sandwiching SiC fibers* between borosilicate glass plates# which were then fused together by heating in air at approximately 850°C for 20 to 30 minutes. The samples were ground to size using standard diamond machining techniques. The four sides were then polished with the final surface finish produced by 0.05μm Al_2O_3 powder. The dimensions, as defined in Fig. 1, were nominally t = w = 6mm and

* SCS-6 Fibers, Avco Corp., Wilmington, MA.

h = 60mm, with a hole radius of 0.8mm. The fibers were placed symmetrically about the central hole with the inner fibers located approximately 9mm from the hole. The specimens were loaded in compression using a screw-driven mechanical testing machine* at a cross-head displacement rate of 0.05 mm/min.

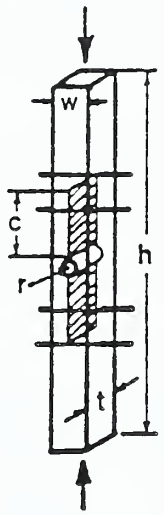

Figure 1 - Double-cleavage drilled-compression fracture mechanics specimen. Compressive load opens cracks above and below centered hole.

Transmitted cross-polarized illumination was used perpendicular to the fiber axis to produce visible strain contours in the specimens. The contours enabled the uniformity of the applied loading to be evaluated, the crack length to be determined, and local strain concentrations associated with the crack-fiber interactions to be detected.

The shape of the crack front and the relative velocity of the growing crack along the specimen were monitored by stress wave fractography.[6] Acoustic waves were propagated through the specimen during crack extension by use of a piezoceramic transducer coupled to the specimen through silicon grease. The acoustic waves produce ripples on the fracture surface which can be observed by optical microscopy in reflected light using differential interference contrast. Each "ripple" marks the position of the crack front at periodic intervals set by the excitation frequency of the transducer, therefore the spacing of the ripples is a measure of the local crack velocity. The transducer was driven with bursts of an 80-90 KHz sine wave at a maximum amplitude of 30 V peak to peak. The burst frequency was 5 Hz; the burst duration was 25% of the low frequency period.

To characterize the mechanical behavior of the fiber/matrix interface in shear, the fibers were pushed through thin sections of the matrix by applying an axial load on the fiber using a Vicker's hardness machine. The hardness tester was instrumented to allow the applied load and the displacement of the diamond indenter to be measured continuously during the testing cycle. Samples were prepared from the broken halves of the DCDC specimens by diamond grinding them to a thickness of approximately 0.85mm perpendicular to the fiber axis and then polishing.

Results and Discussion

A view of a DCDC specimen under load in cross-polarized transmitted light which illustrates the type of qualitative observations that could be made is shown in Fig. 2. The strain contours are symmetric about the center line of the specimen indicating that the specimen is well aligned. The crack emanating from the central hole is seen edge-on with the crack tip located at the center of the hour-glass shaped pattern formed by the strain contours. At this point in the test the crack tip has already moved past the first fiber and is now between the inner and outer fibers. A change in contrast indicating a region of localized strain could be observed in the area where the fiber intersects the crack, demonstrating that the fiber was bridging the crack and exerting a closure force across the crack faces. This feature disappeared following further crack growth, suggesting that the fiber broke at some distance behind the crack tip.

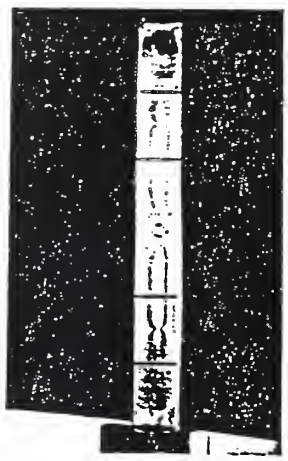

Figure 2 - View perpendicular to fiber axes of DCDC specimen under load. Strain contours are visible by virtue of the transmitted cross-polarized illumination.

An optical micrograph of a fracture surface in the region about the inner fiber, taken with differential interference contrast, is shown in Fig. 3. The fiber axis is perpendicular to the plane of the photograph. The light and dark bands visible under these imaging conditions represent "snapshots" of the position and shape of the crack front at periodic intervals. With a constant excitation frequency applied to the piezoceramic transducer, closely spaced bands indicate slow crack growth, while widely spaced bands reflect regions of more rapid crack propagation. It can be seen that the crack front bowed around the fiber which was bridging the crack before the center portion broke away and accelerated to reform a more nearly straight front. A scanning electron micrograph of the same area (Fig. 4) shows that after bowing around the fiber the two sides of the crack did not meet on the same plane. Fracture of the ligament which formed between the two crack planes was necessary before a continuous crack-front could reform. The scallop-shaped chips around the fiber occurred during fiber pullout. From the indications of bridging which could still be observed in transmitted polarized illumination after the crack had propagated well beyond the fiber,

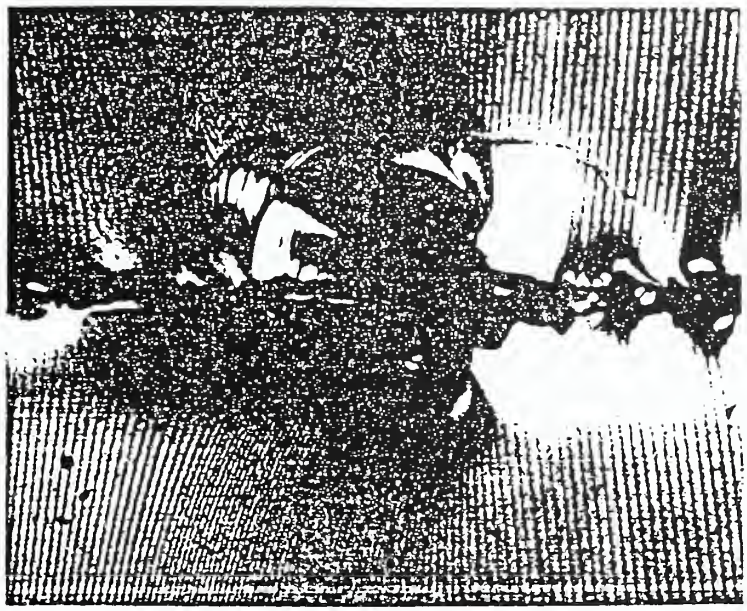

Figure 3 - Optical micrograph of a region of the fracture surface centered about a reinforcing fiber. Differential interference contrast reveals the periodic surface undulations caused by the applied acoustic waves.

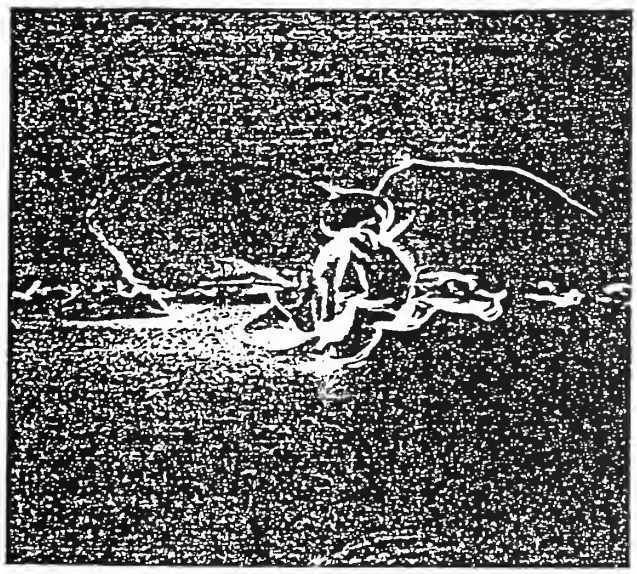

Figure 4 - Scanning electron micrograph of area shown in Fig. 6. The remnant of the glass ligament formed as the crack swept around the fiber can be seen to the left of the fiber.

The quantitative information obtained from the tests is based on stress intensity factor analyses of the DCDC specimen[5-8] which indicate that for a wide range of crack lengths the stress intensity factor (K_{app}) due to the remotely applied compressive load (σ_{app}) is well described as a linearly decreasing function of crack length (c). The expression

$$\frac{\sigma_{app}\sqrt{r}}{K_{app}} = \alpha\frac{c}{r} + \beta \qquad (1)$$

where r is the radius of the center hole in the DCDC specimen, was used to calculate K_{app} from the applied load and crack lengths measured from photographs such as shown in Fig. 2. The constants α and β were evaluated empirically by testing specimens of known K_{IC}. In Fig. 5 the calculated K_{app}, with α=0.151 and β=2.158, is plotted versus c/r for several specimens. Assuming that the crack is growing at a constant stress intensity, $K_{tip} = K_{IC}$ for the glass matrix (0.77 $MPam^{1/2}$)[5], the increase in the calculated K_{app} for crack lengths beyond the fiber position reflects the contribution to the total stress intensity of the closure force exerted by the bridging fiber (K_{fib}):

$$K_{tip} = K_{IC} = K_{app} + K_{fib} \qquad (2)$$

or

$$K_{app} = K_{IC} - K_{fib} \qquad (3)$$

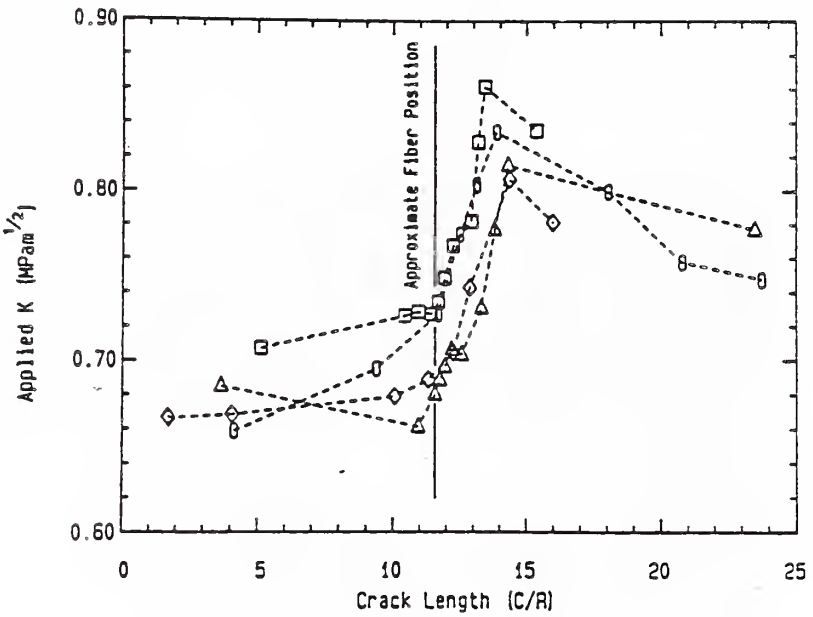

Figure 5 - Plot of applied K due to remotely applied compressive load versus crack length showing relative position of the reinforcing fiber.

The measured crack lengths used to construct Fig. 5 are through thickness averages of the crack length along the crack front. In unreinforced specimens such measurements are adequate since the crack front is nearly straight. However, as seen in Fig. 3 the crack front is curved in the region near the fiber, therefore analysis of these results should incorporate this feature. Assume that the crack front assumes a profile such

curvature must arise from the form of the expression for K_{fib}. The stress intensity factor along a straight crack front due to a point closure force, F, acting at a distance, x, behind the crack tip is given by[10]:

$$K_I = - \frac{\sqrt{2}\ F}{(\pi\ x)^{3/2}} \left(\frac{x^2}{x^2 + z^2} \right) \tag{4}$$

where z describes the position along the crack front (Fig. 6). Substitution of Eq. 4 for K_{fib}, with F taken as the bridging force due to the fiber, and Eq. 1 for K_{app} in Eq. 2 results in an expression which describes contours in the x-z plane (the fracture surface) where $K_{tip} = K_{IC}$ for given values of σ_{app} and F,

$$K_{tip} = \frac{\sigma_{app}\sqrt{r}}{\alpha\frac{x}{r} + \alpha\frac{a}{r} + \beta} - \left(\frac{\sqrt{2}\ \sqrt{x}\ F}{\pi^{3/2}\ (x^2 + z^2)} \right) \tag{5}$$

where a is the distance from the edge of the center hole to the fiber. It is difficult at this time to estimate the error involved in applying Eq. 4 to a curved crack front. Near the fiber, where the crack front curvature is large, Eq. 4 may overestimate K_{fib} by as much as a factor of two or three. The approximation of F as a point force also becomes inadequate within a few fiber radii of the fiber location. Farther from the fiber, where the change in x becomes small with respect to z along the contours of constant K_{tip}, the error should be modest. With an appropriate value of F, it should therefore be possible to account for the observed crack lengths and crack front profiles as a function of the applied stress.

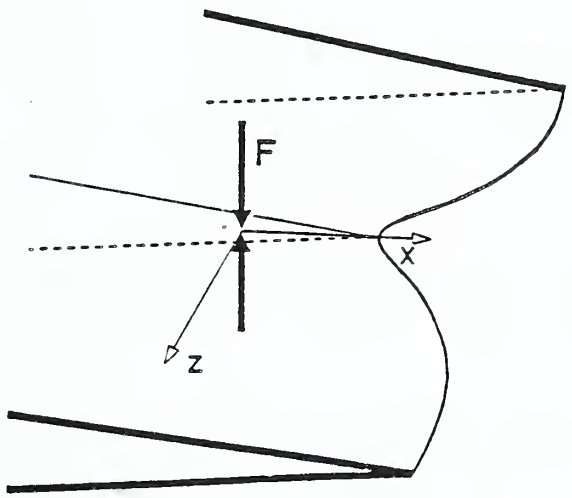

Figure 6 - Schematic illustration of the bowed crack-front profile showing the x-z coordinate system defined on the fracture surface with origin located at the position of the closure force, F.

The closure force is transferred from the fiber to the matrix through shear tractions acting across the fiber/matrix interface. Therefore the closure force exerted across the crack surfaces is controlled by the interfacial properties. To independently evaluate the response of the interface to applied shear stresses an instrumented hardness machine was used to push the fibers through thin sections fabricated from the broken halves of the DCDC specimens. Measured load-displacement curves for two fibers are shown in Fig. 7. The load-displacement records for these tests typically showed a maximum in the applied load followed by an abrupt drop to a plateau load nearly constant over several micrometers of displacement. The increase in load beyond the plateau results from the indenter making contact with the matrix surrounding the fiber. The customary interpretation of this type of result is that the peak applied load corresponds to the applied shear stress required for debonding (τ_{db}) and the plateau load to the stress for frictional sliding (τ_f). Observed values of τ_{db} ranged from 0.8 to 1.0 MPa and of τ_f from 0.4 to 0.7 MPa. An estimate of the magnitude of F is obtained by multiplying τ by the interfacial area, i.e. $F = (\pi\ D\ w/2)\ \tau$.

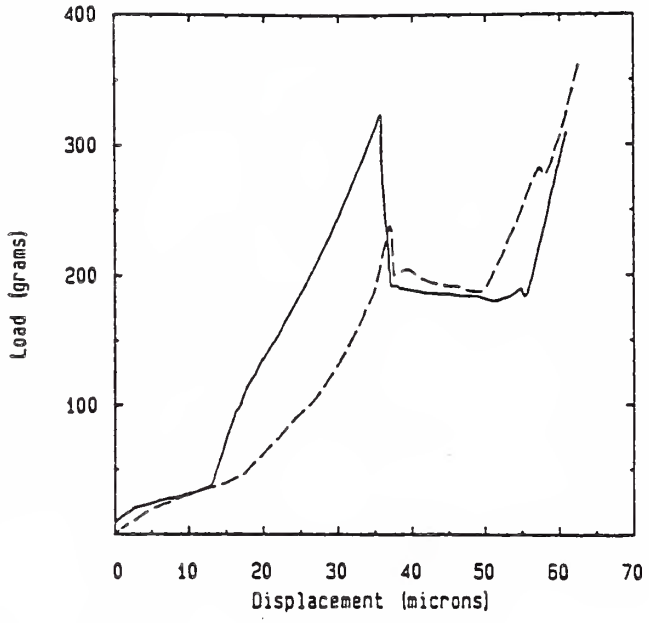

Figure 7 - Curves showing axial load applied to the end of a fiber by the Vicker's indenter versus the displacement of the indenter. The abrupt load drop occurs as the fiber begins to slide through the glass matrix.

Contours of $K_{tip} = K_{IC}$ given by Eq. 5 with F = 0.7N for several levels of applied stress are shown in Fig. 8, where the point force is located at the origin. The shape of the calculated constant K_{tip} contours have the same general shape as the crack front profiles shown in Fig. 3, suggesting that the character of the bridging interaction is fairly well described by Eq. 4. The spatial extent of the calculated interaction is also in fair agreement with that observed, indicating that the magnitude of the trial bridging force is of the correct order. However, in the region near the fiber, where the interactions are strongest, the calculated contours do not describe the experimental observations very well. This may be due to the assumption of

From the results of the indentation experiments it is clear that the force exerted by the fiber varies with the relative displacement of the fiber and the matrix. The bridging force will therefore depend on the debonded length and the crack opening displacement (u). In principle the dependence on crack opening displacement could be introduced into Eq. 4 by taking $F = f(x)$. For example, when a simple frictional sliding resistance (τ_f = constant) can be used to describe the resistance to shear of the interface, F increases with $\sqrt{u}$ (i.e. $F\alpha(u^{1/2}))^{3.4}$. Assuming $u\alpha(x^{1/2})$ would then give $F\alpha(x^{1/4})$. Substitution of such an expression for F in Eq. 6 may yield better agreement with the observed crack front contours. However, several other factors influence the shape of the contours in the region near the fiber. The importance of debonding relative to frictional slippage, the debonded or slippage length, and the errors involved in applying Eq. 4 to this situation can also affect the agreement between the calculated and observed contours. The work now in progress is concentrated on assessing the relative importance of these factors.

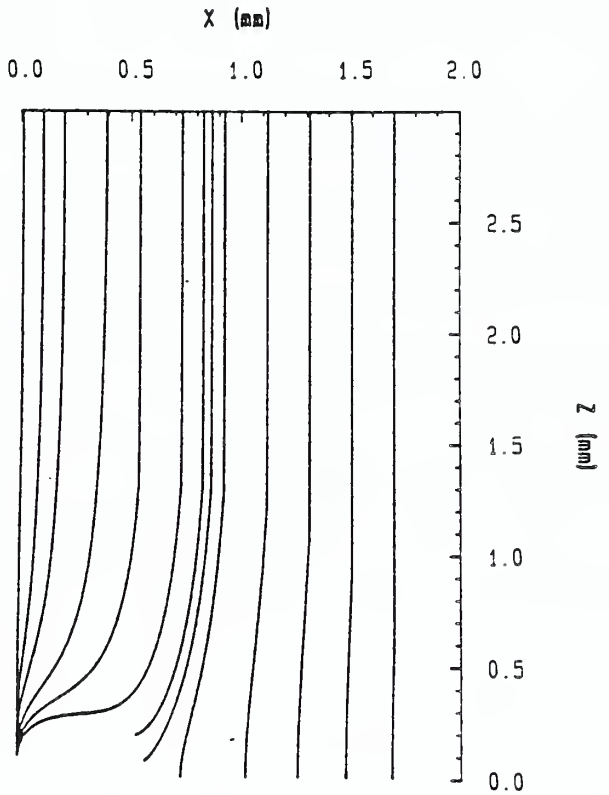

Figure 8 - Contours of constant K_{tip} on the x-z plane (the fracture surface) calculated using Eq. 5 for several values of σ_{app} with F = 0.7N. Each contour, from left to right, corresponds to a larger σ_{app}. The point force (the fiber) is located in the lower left corner (x = 0, z = 0). The area represented would extend from the center line of the DCDC specimen at z = 0 to the specimen edge at z = 3.0.

References

1. T. S. Cook and F. Erdogan, "Stresses in Bonded Materials with a Crack Perpendicular to the Interface", Int. J. Engng. Sci., 10 (1972) 677.

2. J. R. Rice and G. C. Sih, "Plane Problems of Cracks in Dissimilar Media", J. Appl. Mech., 32 (1965) 418.

3. D. B. Marshall, B. N. Cox, and A. G. Evans, "The Mechanics of Matrix Cracking in Brittle-Matrix fiber Composites", Acta Metall., 33 (1985) 2013-2021.

4. D. B. Marshall and A. G. Evans, "Tensile Failure of Brittle-Matrix Fiber Composites", Proceedings of the 5th International Conference on Composite Materials, ICCM-V, ed. W. C. Harrigan, J. Strife, and A. K. Dhingra (Warrendale, PA: The Metallurgical Society, 1985), 557-568.

5. C. Janssen, "Specimen for Fracture Mechanics Studies on Glass", Proceedings of the Xth International Congress on Glass (Kyoto, Japan: The Ceramic Society of Japan, 1974), 23-30.

6. H. Richter, "Crack Propagation in Glass Under Liquids in an Intermediate Range of Crack Velocities", Strength of Inorganic Glass, ed. C. R. Kurkjian (Plenum Publishing Corp., 1985), 219-229.

7. J. H. Henry, "Energie d'Avancement de Fissure, G, pour une Plaque Percee d'un Trou Soumise en Compression', Mechanics Research Communications, 10 (5) (1983) 253-257.

8. C. G. Sammis and M. F. Ashby, "The Failure of Brittle Porous Solids Under Compressive Stress States", Act Metall., 34 (1986) 511-526.

9. W. E. Warren, "Theoretical Analysis of the Double Cleavage Drilled Compression Specimen", Int. Journal of Fracture, 33 (1987) 223-325.

10. H. Tada, P. C. Paris, and G. R. Irwin, The Stress Analysis of Cracks Handbook (Hellertown, PA: Del Research Corp., 1973).

Ceram. Eng. Sci. Proc., 9 [7-8] pp. 627-634 (1988)

Determination of the Interface Strength in Glass-SiC Composites via Single Fiber Tensile Testing

U. V. DESHMUKH

Department of Materials Engineering
Drexel University
Philadelphia, PA 19104

T. W. COYLE

Ceramics Division, Inst. Materials Sci. and Eng.
National Bureau of Standards
Gaithersburg, MD 20899

Single fiber tensile tests were performed on Borosilicate[§] glass-SiC-fiber composites to measure the interfacial shear strength. Samples were prepared by sandwiching SiC fibers, 140 μm in diameter between borosilicate glass plates fused together by heating to 750°C under a dead weight corresponding to about 1.5 psi. The interface was varied by using fibers with different surface layers. The samples were tested in tension and the load-displacement curves recorded. The interface shear stress has been calculated as the maximum force divided by the initial contact area. For this system, interface shear stresses in the range 6-14 MPa have been measured.

Introduction

The structure and properties of the fiber-matrix interface play a major role in the mechanical and physical properties of composite materials. The interface largely determines the fracture toughness of composite materials. Composites with weak interfaces have relatively low strength and stiffness but higher resistance to fracture, whereas materials with stronger interfaces have high strength but low resistance to fracture, the effect being related to debonding and pullout of fibers from the matrix during crack propogation.[1]

The strengths of fiber-matrix interfaces have been measured by many different techniques, but single fiber pullout tests give the most direct measure of the interface shear strength.[2-4] Resistance to debonding and pullout process is a function of the fiber-matrix interfacial bond strength and the interfacial bond area. A very good review of the existing theories of stress analysis during pullout experiments is given by Gray.[5] Most of the theoretical work is based on the shear-lag analysis of Cox[6] which was subsequently modified by Greszczuk[7] and Lawrence[8] for the case of brittle matrices loaded elastically. To simplify the stress analysis most authors have assumed that the interface is strongly bonded to start with. This may not necessarily be true, for instance, in the LAS-Nicalon™ composites it has been shown

[§]Corning 7740, Corning Glass Works, Corning, NY.
*SCS-6 Fibers, AVCO Corporation, Lowell, MA.
™Nicalon manufactured by Nippon Carbon Co., Japan.

that the interfacial bond is indeed weak.[9-10] The resistance to pullout in that case is mainly frictional.

A model system of Borosilicate[5] glass and SiC[*] fibers was used in this work. The fiber has a carbon rich layer on the outer surface and therefore it is argued that the fiber may not bond to the glass. Thus the resistance to pullout is mainly frictional arising from the difference between coefficients of thermal expansion of the two components. The interface shear strength in this case can be estimated as the maximum pullout force divided by the contact area. We realize that this is a very simplistic model, but nevertheless feel that it may serve as a good first approximation.

Experimental Procedure

The samples were fabricated by sandwiching SCS-6 SiC fibers between Borosilicate glass plates and heating them under a dead weight as shown in Fig. 1. Fibers were placed between two plates with different embedded lengths. The assembly was heated in a vacuum hot press to 750 °C at a heating rate of 10 °C/min in helium atmosphere. The vacuum hot press was used mainly for heating rather than pressing. Helium was kept flowing throughout the fabrication of the samples to prevent oxidation of fibers. The samples were held at temperature for 30 min and furnace cooled. The dead weight corresponded to about 1.5 psi pressure.

After removal from the furnace, the slides were waxed to another glass plate and cut into individual tensile samples using a high speed diamond saw; holes were drilled along the fiber axis. It is important to get good alignment of the holes with the fiber axis to minimize bending forces during testing. A schematic of the sample is shown in Fig. 2. The tensile samples were observed optically in transmission mode to check for any defects at the interface. In most cases no bubbles were seen at the interface indicating that there was no reaction between glass and fibers. The embedded length was measured using an optical microscope, however the exact position of fiber when it emerges from between the plates cannot be determined accurately, so the optically measured embedded length is only approximate.

Individual tensile samples were loaded in uniaxial tension on a table top Instron[#] machine, using a 5 kg load cell. The samples were gripped using swivel hooks. The swivels have two ball joints that facilitated alignment of the fiber. Samples were pulled at a rate of 0.5 mm/min and the chart speed was 40 mm/min. In some instances when the fiber had pulled out a certain distance the straining was stopped and the fiber unloaded. The pullout distance was measured optically and then checked with the chart. It was observed that the chart gave accurate recording of the pullout distance. Hence the initial embedded length was measured from the chart.

Results

The data from the pullout tests are obtained in the form of load vs chart units which can be converted to force vs displacement, where displacement indicates movement of the crosshead. Typically two types of curves were observed as shown in Figs. 3 and 4. In both cases the load increased linearly with displacement until the pullout began. In the first case (Fig. 3), further pullout was accompanied by

---

[*]Instron Corp., Canton, MA.

a decrease in load and the process continued smoothly until the fiber pulled out completely. In the second case (Fig. 4), at the instant of pullout there was a sharp drop in load; however, the load increased again to a value just lower than the previous, when the fiber pulled out again. This process continued until the loads dropped substantially and then for the remaining part the fiber pulled out smoothly. This phenomenon has been reported in the literature[11,12] and has been called the "stick-slip" friction. Interestingly whenever the fiber pulled out it made a clicking noise. This particular observation was also reported by Griffin for the Borosilicate-SCS-6 system.[13]

The maximum force required for pullout vs embedded length as measured from the chart for four different sets of samples is shown in Fig. 5. SCS-6 and SCS-6 #2 have a carbon rich layer on the outer surface. In the case of SCS-6 P the layer is present only partially along the circumference, whereas it is absent in SCS-6 UN. The force required for pullout increases with increasing embedded length as long as the fiber strength is not exceeded. The maximum interfacial shear stress was calculated as the force divided by the initial contact area. The results are shown in Fig. 6. The error bars correspond to the errors in measurement of load and the embedded length. Typically there is about 15% error in the interfacial shear stress as calculated by the above method.

Attempts were also made to monitor the interfacial shear stress during the pullout test. To do this the pullout length and hence the instantaneous embedded length was calculated from the displacement of the crosshead. The interfacial shear stress was then calculated as the force divided by the instantaneous contact area. The interfacial shear stress decreases with decreasing instantaneous embedded length as can be seen from Fig. 7. The interfacial shear stress increases in the end, but we believe that the data in that region are unreliable since the embedded length is extremely small and therefore bending moments may have been introduced leading to an apparent increase.

Discussion

The maximum force required for pullout is proportional to the embedded length as long as the fiber strength is not exceeded. If the interface bond is purely frictional with a constant coefficient of friction, then the maximum force required to pullout should vary linearly with the embedded length. Samples marked SCS-6 and SCS-6 UN seem to follow that trend. The variation in embedded length for SCS-6 #2 is not large enough to draw any conclusions. Although SCS-6 and SCS-6 #2 are nominally the same fibers, there is a difference in maximum pullout force, indicating that processing may play a role in determining the interface properties.

Since the interfacial shear stresses are obtained by calculating the embedded length from the chart some discussion on this measurement is warranted. The schematic of a pullout curve is shown in Fig. 8 with a superimposed line corresponding to the fiber force-displacement curve. If the elastic modulus of the machine and the grips were infinite, the slope of the loading part of the force-displacement curve should correspond to the fiber elastic modulus. Any deviation from that therefore has to be due to the displacement of the setup in terms of the fixtures. Also there is a free fiber length between the glass pieces. When the sample is loaded, this section will elastically deform; the elastic displacement is a function of applied force and the free length. Hence the total displacement during loading will be a sum of the fiber and machine (fixtures etc.) displacements. After the fiber starts to pull out there is a decrease in force due to a decrease in contact area.

The fixtures and the fiber then start to unload, and clearly at reduced loads the elastic displacement is less. Therefore, the pullout displacement will be given by that between the loading and the unloading points at that force. Two things should be noted here: one, the free length is constantly changing as the fiber pulls out, and two, the initial embedded length is given by the displacement at zero load. The instantaneous embedded length at any given load can therefore be calculated as the difference between the initial embedded length and the pullout length. In order to correctly account for the pullout displacement at intermediate loads the changing free length will have to be considered. The initial embedded length however remains unchanged.

The interfacial shear stress at the instant of pullout is expected to be constant and independent of the embedded length when the resistance to pullout is purely frictional. The shear stress is mainly a function of the normal stress acting at the interface which arises from the difference between coefficients of thermal expansion (CTE) of the glass and the fiber. In order to estimate the residual stresses at the interface, the glass transition temperature and the CTEs of the components at that temperature must be known. The CTE of glass may be assumed to be isotropic, but there may be some anisotropy in the CTE of the fiber due to the presence of graphite core and the directionality of SiC grains. Therefore the CTE of the fiber in the radial direction is more important.

The interface shear stress does seem independent of the embedded length for the SCS-6, SCS-6 #2 and SCS-6 UN samples. The SCS-6 P has the highest interface shear stress followed by SCS-6 UN and SCS-6. The uncoated fiber would be expected to exhibit higher interfacial shear stress due to surface roughness, however the uneven surface condition of the partially coated fibers may have lead to higher interfacial stresses. The SCS-6s should have same interface shear strength since they were fabricated identically and it is not clear why there is a difference. It should be pointed out that the error in the experiments is typically about 15%, and therefore the small differences in the measured shear strengths may not be real.

The interface shear stress was monitored throughout the pullout test by calculating the instantaneous embedded length as enumerated previously. The shear stress does not remain constant throughout the test. In all cases it decreased with decreasing embedded length. As stated before, if the resistance to pullout is frictional then the shear stress should have remained constant. The residual normal stress at the interface is independent of the embedded length and is determined by processing conditions only. The interface shear stress can be looked upon as a product of this normal stress and a coefficient of friction. The assertion that shear stress is constant relies on the assumption that the coefficient of friction is a constant. It may be argued that the friction between the glass and fiber could arise from asperities on the fiber surface. As the fiber is progressively pulled out, these asperities may be getting smoothened out thereby reducing the coefficient of friction.

The "stick-slip" friction has been observed mainly in the case of fibers with smooth surfaces. It appears that a threshold stress is built up at the interface before the fiber pulls out again. The reasons for this phenomenon are not quite clear as yet. The accoustic emission during pullout is probably the release of excess strain energy stored in the free length of the fiber when the fiber reloads.

Conclusions

1. Single fiber pullout tests can be used to evaluate the interface shear strength in ceramic matrix composites. Greater care is required when testing with shorter embedded lengths and weaker fibers.

2. For the SiC-Borosilicate glass system, interface shear strengths of the order of 6-14 MPa, measured as maximum force/contact area have been observed.

3. The nature of bonding at the fiber/glass interface appears to be mainly frictional for the SiC-Borosilicate glass system.

Acknowledgments

The authors would like to thank Dr. S. W. Freiman, Dr. M. J. Koczak, and Dr. M. Barsoum for helpful discussions. We are grateful to Dr. S. G. Fishman at Office of Naval Research for the support through contract #N00014-86-F-0096.

References

[1]D. Hull, *An Introduction to Composite Materials*, Cambridge University Press, 1980.

[2]B. Harris, J. Morley, and D. C. Philips, "Fracture Mechanisms in Glass-Reinforced Plastics," *J. of Mat. Sci.*, Vol. 10, pp. 2050-2061, 1975.

[3]A. Takaku and R. G. C. Arridge, "The Effect of Interfacial Radial and Shear Stress on Fiber Pullout in Composite Materials," *J. Phys. D: Appl. Phys.*, Vol. 6, pp. 2038-2047, 1973.

[4]M. R. Piggott, A. Sanadi, P. S. Chua, and D. Andison, "Mechanical Interactions in the Interphasial Region of Fiber Reinforced Composites," pp. 109-121 in *Composite Interfaces*. Ed. by H. Ishida and J. L. Koenig, Elsevier Publishing Co. Inc., (1986).

[5]R. J. Gray, "Analysis of the Effect of Embedded Fiber Length on Fiber Debonding and Pullout from an Elastic Matrix," *J. of Mat. Sci.*, Vol. 19, pp. 861-870, 1984.

[6]H. L. Cox, "The Elasticity and Strength of Paper and Other Fibrous Materials," *Brit. J. Appl. Phys.*, Vol. 3, pp. 72-79, 1952.

[7]L. B. Greszczuk, "Theoretical Studies of the Mechanics of the Fiber-Matrix Interface in Composites," pp. 43-58, in *Interfaces in Composites*, ASTM STP 452, American Society for Testing and Materials, (1969).

[8]P. Lawrence, "Some Theoretical Considerations of Fiber Pullout from an Elastic Matrix," *J. of Mat. Sci.*, Vol. 7, pp. 1-6, 1972.

[9]J. J. Brennan and K. M. Prewo, "Silicon Carbide Fiber Reinforced Glass-Ceramic Matrix," *J. of Mat. Sci.*, Vol. 17, pp. 2371-2383, 1982.

[10]D. B. Marshall and A. G. Evans, "Failure Mechanisms in Ceramic-Fiber/Ceramic-Matrix Composites," *J. Amer. Ceramic Society*, Vol. 68, No. 5, pp. 225-231, 1985.

[11]P. S. Chua and M. R. Piggott, "The Glass Fiber-Polymer Interface: II—Work of Fracture and Shear Stresses," *Composites Sci. and Tech.*, Vol. 22, pp. 107-119, 1985.

[12]L. S. Penn and S. M. Lee, "Interpretation of the Force Trace for Kevlar/Epoxy Single Filament Pullout Tests," *Fiber Sci. and Tech.*, Vol. 17, pp. 91-97, 1982.

[13]C. W. Griffin, private communication, 1988.

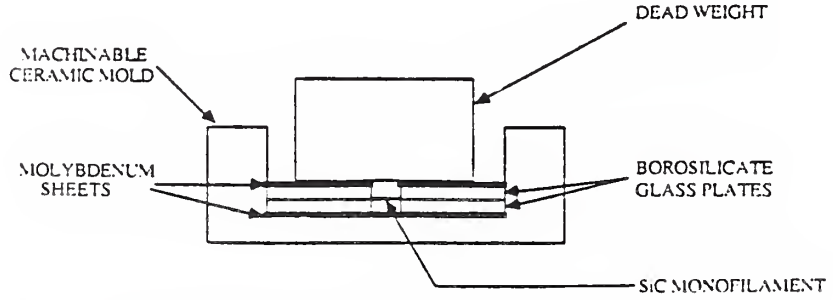

Fig. 1. Schematic of the sample making die assembly.

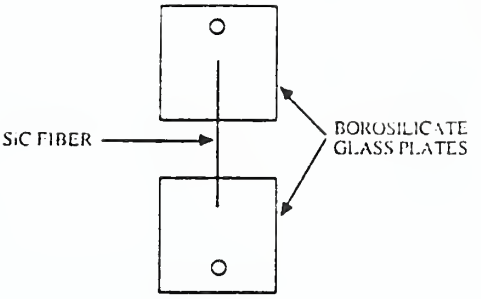

Fig. 2. Schematic of the individual sample.

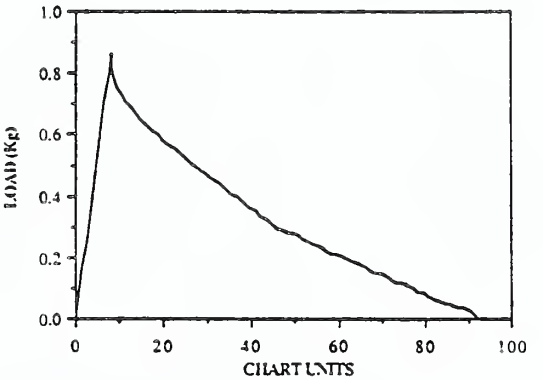

Fig. 3. Load-chart unit curve for a sample pulling out smoothly.

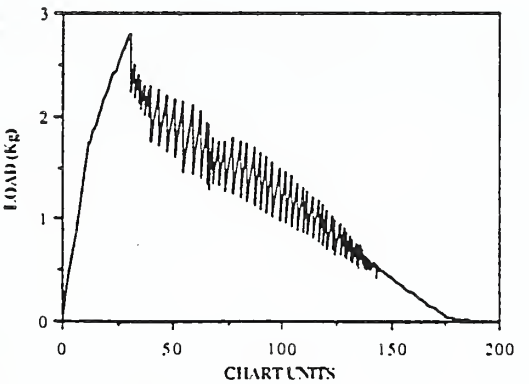

Fig. 4. Load-chart unit curve for a sample exhibiting "stick-slip" behavior.

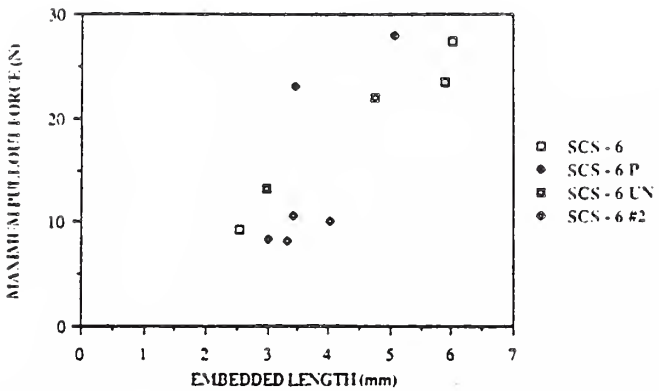

Fig. 5. Maximum pullout force vs embedded length for various sets. SCS-6 has a carbon rich layer on the outer surface, SCS-6 P has a partial covering of this layer, while in SCS-6 UN this layer is absent. SCS-6 and SCS-6 #2 are the same fibers.

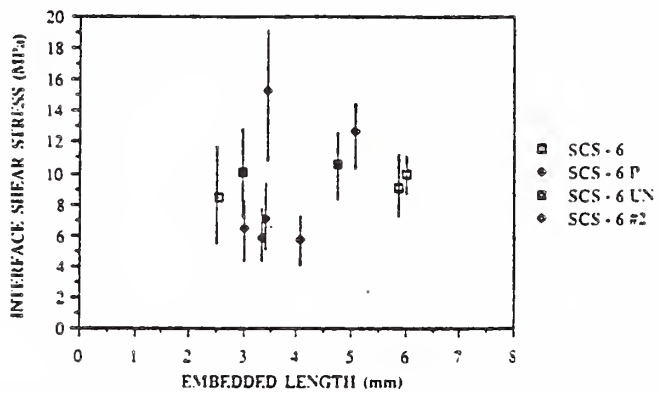

Fig. 6. Interfacial shear stress as a function of embedded length. Bars show the error in measurement. SCS-6 has a carbon rich layer on the outer surface, SCS-6 P has a partial covering of this layer, while in SCS-6 UN this layer is absent. SCS-6 and SCS-6 #2 are the same fibers.

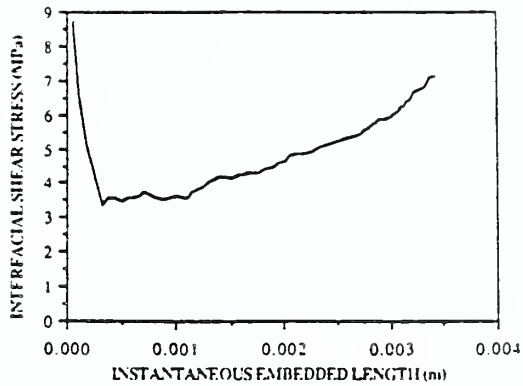

Fig. 7. Plot of interfacial shear stress throughout a single test as a function of instantaneous embedded length.

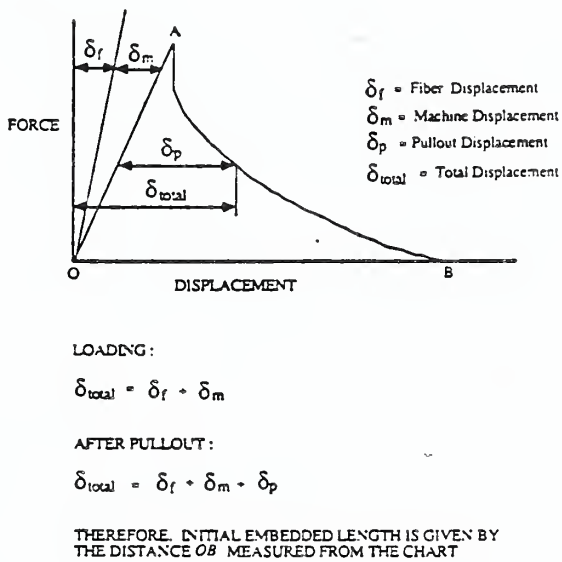

Fig. 8. Schematic showing the measurement of initial embedded length from the force-displacement curve.

Ceram. Eng. Sci. Proc., 9 [7-8] pp. 687-694 (1988)

Interfacial Chemistry of Mullite-Mullite Composites

ORI YEHESKEL,* MARI LOU BALMER, AND DAVID C. CRANMER

Ceramics Division
National Bureau of Standards
Gaithersburg, MA

Interfacial chemistry of mullite fiber reinforced-mullite matrix composites was examined using SEM/EDX and scanning AES. All the fibers bond strongly to the matrix and exhibit no sliding during a fiber push-in test. Excess Si over Al is found at the fiber-matrix interfaces. AES results show the carbon layer is nonuniform and in some cases less than 30 nm thick.

Introduction

The key to obtaining strength and toughness in ceramic matrix composites lies in the ability to control the chemistry and properties of the fiber-matrix interface. In these materials, the bond between the fiber and matrix should be such that the fibers are difficult to pull out of the matrix but not so strong that cracks propagate unimpeded across the fibers and matrix. Carbon and boron nitride coatings have been shown to provide the necessary interfacial properties.[1,2]

Mullite ($3Al_2O_3 \cdot 2SiO_2$) has potential application as a radome material[3] but one deficiency[4] in the monolithic form is its low fracture toughness (K_{Ic}). Improvement of K_{Ic} from 2.2 MPa·m$^{1/2}$ to 4.7 MPa·m$^{1/2}$ was reported[4] through the addition of 20 vol% SiC whiskers. Although a considerable improvement, the addition of 20 vol% SiC whiskers may adversely affect the dielectric properties. The present study was undertaken to examine the possibility of producing mullite matrix composites reinforced by continuous mullite fibers.

Experimental Procedures

Three different mullite fibers were used in this study: Nextel 480, Nextel 440, and carbon-coated (by a CVD process) Nextel 440.† Fiber phase composition was determined by X-ray diffraction. Additional characterization was done using SEM with EDX analysis. Carbon-coated Nextel 440 fiber was examined in a scanning Auger microprobe. The composites were fabricated by laying each set of fibers between previously cold-pressed (25 MPa) mullite powder bars,‡ which were then cold-pressed (50 MPa), wrapped with Mo foil, and hot pressed in a graphite die (Ar atmosphere of 0.1 MPa at 1465 °± 10 °C, 27 MPa, 1 hour). The three resulting composites were separated from one another with a diamond wafering blade. Density was determined by Archimedes' method in distilled water. Microhardness of the fibers and matrices was determined using the method of Marshall,[5] which is an indentation push-in test, at loads of 0.5, 1, and 2 N. The composites were examined in the SEM after being coated with a thin layer of carbon to reduce charging and permit data acquisition for chemical microanalysis by EDX.

*On leave from NRCN, Israel.
†3M Corp., Ceramic Materials Dept., St. Paul, MN.
‡High Purity Mullite 193-CR, Baikowski International, Charlotte, NC.

Results and Discussion

Indentation

Examination of the fiber indentations showed that no movement had occurred. In many cases, cracks which initially developed in the dense fibers propagated from the indentation site into the less dense matrix, suggesting that the bond between the fiber and matrix is a strong chemical bond. Figure 1(*A*) shows an indent in the middle of a carbon-coated 440 fiber, where blunting of the cracks in the matrix can be seen. Figure 1(*B*) shows 1 N indent on one fiber in a 440 bundle, where the cracks extend into the matrix and on into the fiber bundle. Figure 1(*C*) shows various 1 N indents in a bundle of Nextel 480 fibers; crack extension is evident. Table I summarizes the hardness values of the fibers and matrices. The hardness of single fibers in the less dense matrix is always less than in the dense fiber bundle. The results show that the hardness increases with decreasing indentation load. Similar findings of increasing hardness with decreasing loads have been reported in ceramics.[6,7] Differences in matrix hardness are probably due to density differences arising from the hot pressing process. The composite density ranges from 82 to 87%. Given the lack of fiber motion, additional chemical information on the fiber-matrix interface is discussed below.

Interface Chemistry

Figures 2(*A–C*) show the X-ray diffraction patterns of the three fibers. Analysis (Table II) shows that the 480 fibers consist of mullite and a minor amount of an amorphous phase. The 440 fibers contain mullite, an amorphous phase, and η-Al_2O_3. The coated 440 contains less amorphous phase and more mullite than does the uncoated 440, suggesting that mullite was formed at the expense of the amorphous phase during coating.

EDX analysis showed that a stoichiometric mullite matrix was not present except in the Nextel 440 fiber-containing sample, all other cases showed an excess of Si over Al. Since the carbon layer may preferentially absorb the Al X-rays, a correction factor (CF) was incorporated into the compositional analyses. The CF was determined by calculating the ratio between the theoretical stoichiometric mullite (28.25 wt% SiO_2) and the calculated SiO_2 wt% content determined from the measured Si value in each matrix. The CF was multiplied by the calculated wt% SiO_2 in the fibers. Al_2O_3 content is assumed to be 100 wt% SiO_2. The corrected values of SiO_2 and Al_2O_3 are shown in Table II.

Uncorrected EDX line scans and corresponding micrographs along a bare Nextel 480 fiber, across two Nextel 480 fibers in the composite, and across one Nextel 440 fiber in the composite are shown in Figs. 3(*A–C*), respectively. Figure 3(*A*) shows a homogeneous distribution of Al and Si along the fiber as well as a systematic variation in Si and Al, representative of an apparent layered structure in the fiber. The scans in Figs. 3(*B*) and 3(*C*) show that the interfaces between fiber and matrix and between fiber and fiber contain larger amounts of Si than Al. Si is probably present as a (boro)silicate, resulting in a strong chemical bond across the interfaces. However, the interface composition was not determined because the precise boron content could not be measured due to interference from the carbon coating.

Figure 4 shows the AES survey scan of the carbon-coated Nextel 440 fiber. In addition to C from the coating, the elements present in the fiber (Si, Al, B, and O) are all evident. The fact that the fiber elements are seen prior to sputtering indicates that the coating is thin ($\leq$30 nm). Survey scans taken at other points do not show the fiber elements without surface removal, indicating a nonuniform

coating. Analysis of the energy peak location[8] shows that Si is present in a covalent environment (Si or SiC) while Al is present in a metallic or carbidic form (Table III). Al is assumed to be present as the carbide. The peak shape of the carbon indicates that it is present as carbidic material, not as a hydrocarbon. Figure 5 shows the depth profile of the coated fiber. The sputtering rate of carbon is about 12.5 nm/min, thus the coating in this location is about 25 nm thick. On sputtering through the surface layer, the carbon concentration increases to a peak, while the Al and O contents decrease and the Si and B contents increase slightly. At depths greater than that corresponding to the carbon concentration peak, the carbon content decreases steadily to a constant value, the Al and O concentrations increase significantly to approximately constant values, and the Si and B contents decrease slightly. After most of the carbon layer has been removed, the variation of Al, Si, and B is systematic, indicative of a layered structure as was seen in Fig. 3(*A*). The depth profile indicates that carbon atoms diffused into the interior of the fiber.

Conclusions

The results of this study showed that the fibers did not move during the push-in test. Cracks extend unimpeded from the fibers to the matrix and from fiber to fiber within fiber bundles. This behavior is indicative of a strong interfacial bond between fiber and matrix and between fiber and fiber. The end result is that no toughening of the mullite material would be expected. The surface chemical composition of the fibers changes from a homogeneous distribution of Al and Si prior to hot pressing to an inhomogeneous, Si-rich material in the studied composites. These interfaces most likely consist of a borosilicate glass composition.

The carbon coating on the Nextel 440 fibers, which was expected to provide the necessary interface properties, was either too thin or too nonuniform to act as the appropriate interface. Auger results showed that the fiber's major constituents diffused through the carbon during the coating process, enabling or enhancing the formation of a strong chemical bond between the fibers and matrix.

Acknowledgments

We would like to thank Dr. Allan Holtz of 3M for supplying the carbon-coated Nextel 440 fibers, to Dr. Alexander Shaprio of NBS/Metallurgy Div. for assisting in the SEM/EDXA work, and to DARPA/DSO for funding this work.

References

[1]B. Bender, D. Shadwell, C. Bulik, L. Incorvati, and D. Lewis III, *Amer. Cer. Soc. Bull.*, 65 [2] 363-369 (1986).
[2]K. M. Prewo and J. J. Brennan, *J. Mat. Sci.*, 15 (1980) 463–468.
[3]D. P. Partlow, W. R. Brose, and C. A. Andersson, AFWAL-TR-85-4152, April 1986.
[4]P. F. Becher, T. N. Tiegs, J. C. Ogle, and W. H. Warwick in Fracture Mechanics of Ceramics, 7: Composites, Impact, Statistics, and High Temperature Phenomena, R. C. Bradt, A. G. Evans, D. P. H. Hasselman, and F. F. Lange, eds., Plenum, New York, 1986, pp 61-73.
[5]D. B. Marshall, *J. Amer. Ceram. Soc.*, 67 [12] C259-C260 (1984).
[6]D. Chakraborty and J. Mukerji, *J. Mat. Sci.*, 15 (1981) 3051-3056.
[7]K. Niihara and T. Hirai, *J. Mat. Sci.*, 12 (1977) 1243-1252.
[8]L. E. Davis, N. C. MacDonald, P. W. Palmberg, G. E. Riach, and R. E. Weber, Handbook of Auger Electron Spectroscopy, 2nd Edition, Physical Electronics Industry, Eden Prarie, MN 1972.

Table I. Vickers Microhardness of Fibers and Matrix (GPa)*

Load (N)	Matrix # 1	Matrix # 2	Matrix # 3	Fiber # 1	Fiber # 2	Fiber # 3
0.5	13.1±1.8	13.7±3.0	8.8±1.0	17.5±2.0	19.7±3.0	17.7±1.5
1.0	10.9±1.0	12.1±1.0	8.7±0.7	15.9±1.3	15.7±0.5	17.7±0.8
2.0	7.6±1.5	9.5±1.0	6.3±0.6	—	—	—

*Matrix (*i*) contains Fiber (*i*).

Table II. Chemical and Phase Composition of Mullite Fibers

Mullite Fibers	Chemical composition Al_2O_3 wt%	SiO_2 wt%	B_2O_3 wt%	Phase composition
Nextel 480				
nominal	70	28	2	Mullite ($3Al_2O_3 \cdot 2SiO_2$)
present study*	70.1±1	29.9±1	nd*	Mullite (VS)‡+Amorphous phase (VW)
Nextel 440				
nominal	70	28	2	Mullite+γ-Al_2O_3
present study*	69.6±1	30.1±1	nd*	Mullite (M-S)+η-Al_2O_3 (S)+Amorphous phase (M-W)
Nextel 440 w/ C				
nominal	70	28	2	Mullite+γ-Al_2O_3
present study*	70.5±1	29.5±1	nd*	Mullite (S)+η-Al_2O_3 (S) +Amorphous phase (W)

*Corrected as explained in text.
*Not detected.
‡VS-Very Strong, S-Strong, M-Medium, W-Weak, VW-Very Weak.

Table III. Auger Peak Locations in Composite vs Handbook Values

Element	Composite location (eV)	Handbook value and environment (eV)*
Si	92	72 (Si), 76 (SiO_2)
	1619	1619 (Si), 1606 (SiO_2)
Al	68	51 (Al_2O_3), 68 (Al)
	1394	1378 (Al_2O_3), 1396 (Al)
C	272	272 (C)
B	179	179 (B)
O	508	503 (MgO)

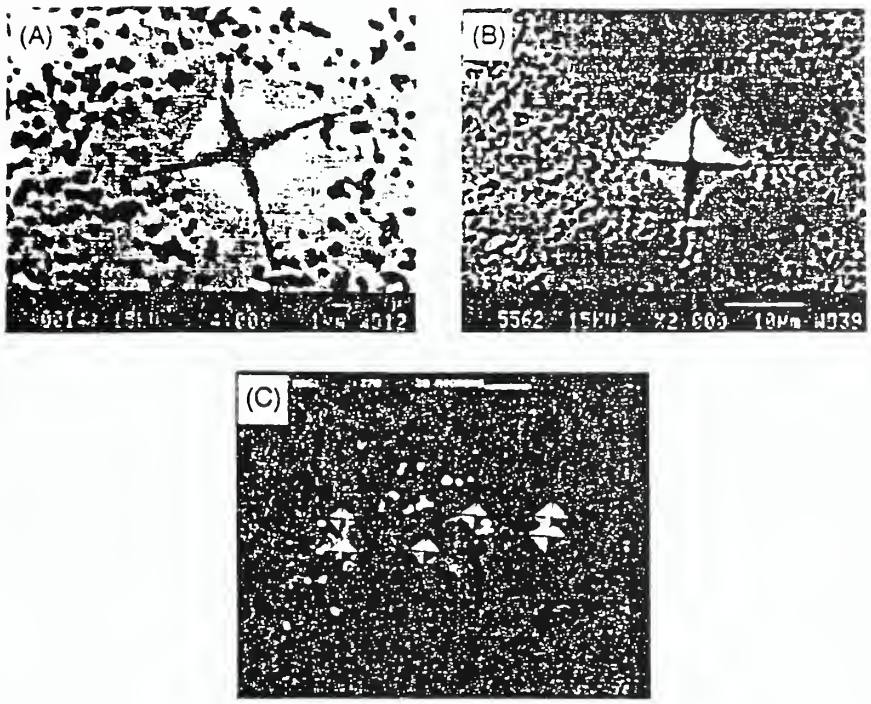

Fig. 1. Micrographs of polished and indented sections: (*A*) carbon-coated Nextel 440, 0.5 N load, (*B*) Nextel 440, 1.0 N load, and (*C*) Nextel 480, 1.0 N load.

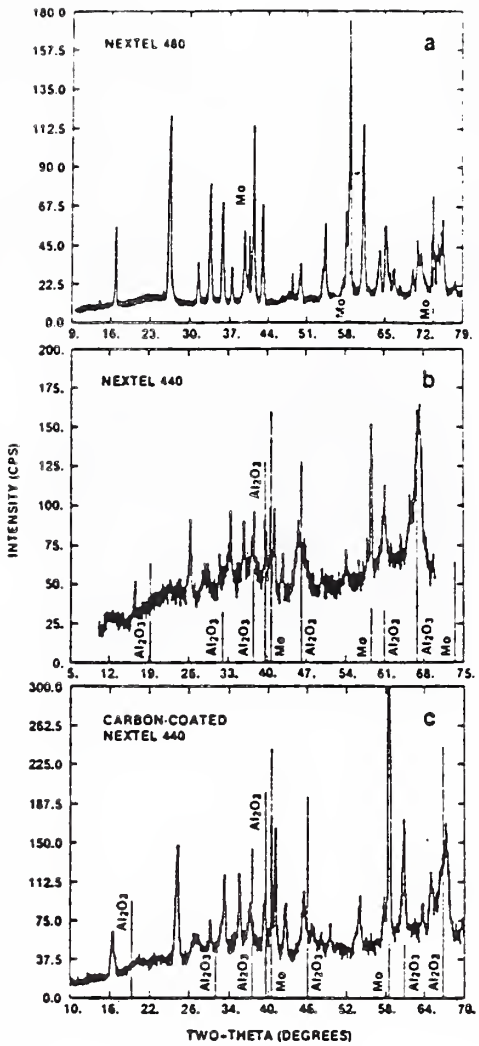

Fig. 2. X-ray diffraction patterns of the fibers on a Mo substrate (unmarked peaks are mullite): (*A*) Nextel 480, (*B*) Nextel 440, and (*C*) carbon-coated Nextel 440.

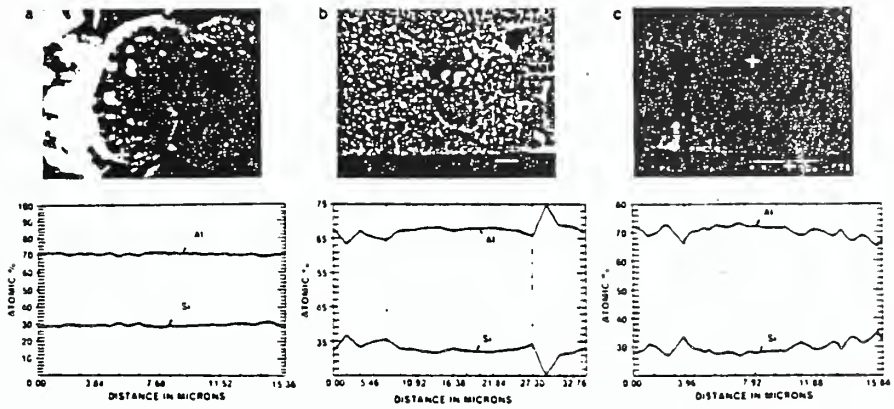

Fig. 3. EDX line scans showing Al and Si concentrations: (*A*) bare Nextel 480 fiber, (*B*) two Nextel 480 fibers in contact in composite, and (*C*) one Nextel 440 fiber in composite.

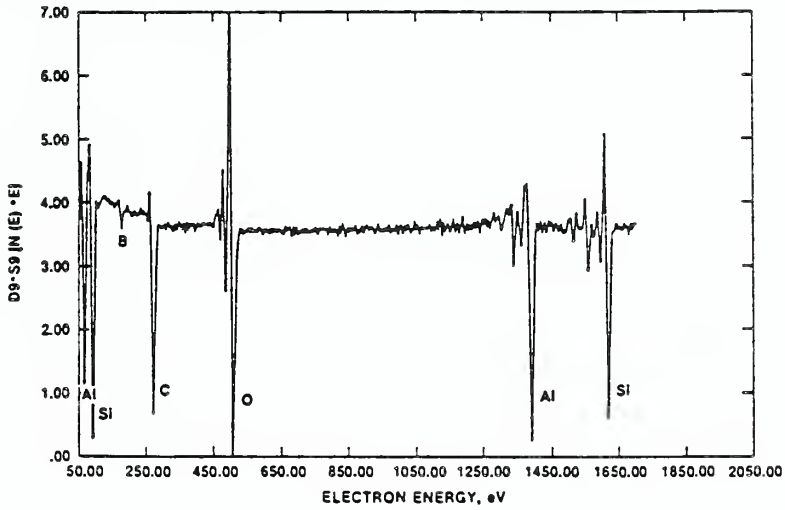

Fig. 4. AES survey scan of carbon-coated Nextel 440 fiber.

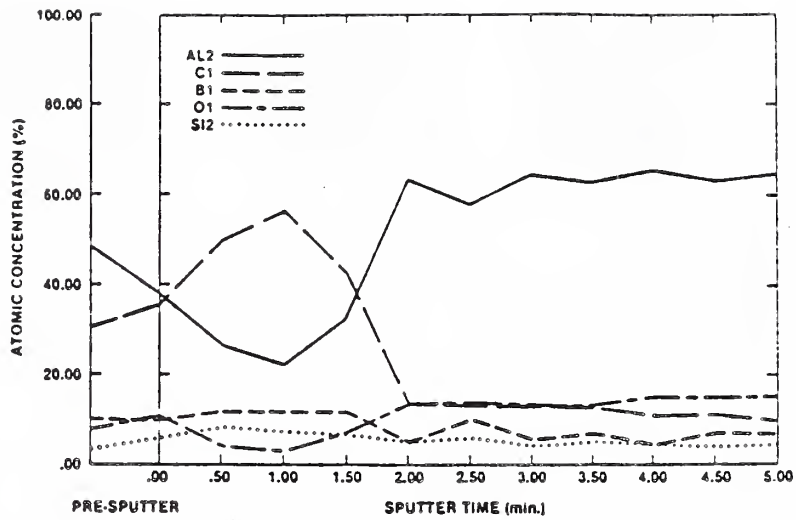

Fig. 5. AES depth profile of carbon-coated Nextel 440 fiber.

EFFECT OF THERMAL EXPANSION MISMATCH ON FIBER PULL-OUT IN GLASS MATRIX COMPOSITES

U. V. Deshmukh*, A. Kanei*, S. W. Freiman** and D. C. Cranmer**
*Department of Materials Engineering, Drexel University, Philadelphia, PA 19104
**Ceramics Division, National Bureau of Standards, Gaithersburg, MD 20899

ABSTRACT

Single fiber pull-out tests can be used to directly measure the fiber-matrix interfacial shear stress in glass matrix composites. The system under investigation consisted of a soda-lime-silica glass matrix containing SiC monofilaments with a carbon-rich surface. The presence of the carbon-rich layer on the surface of these fibers makes them non-wetting to most glasses; hence the fibers are held in the matrix only by frictional forces acting at the interface. The mechanical gripping responsible for this force can be changed by manipulating the glass matrix/fiber thermal expansion coefficient mismatch. Frictional stresses (τ) and friction coefficients (μ) obtained for SiC monofilaments in a soda-lime-silica glass matrix were compared with previously obtained data on a borosilicate glass matrix (τ = 2-3 MPa, μ = 0.72 ± 0.36). For the soda-lime-silica system, τ's of 4-20 MPa and μ of 0.10 ± 0.03 were obtained. τ in the soda-lime-silica system is higher due to the larger difference in thermal expansion mismatch between the fiber and matrix. The differences in μ may be due to lubrication effects caused by water at the fiber-matrix interface.

INTRODUCTION

Strengths of fiber-matrix interfaces have been measured by several different techniques, but single fiber pull-out tests give the most direct measure of the interface strength [1-3]. Depending on the nature of the interaction (chemical and/or mechanical) between the fiber and the matrix, a single fiber pull-out test gives information about both the debonding and pull-out processes occurring in composites. However, single fiber pull-out tests have been used for glass matrix systems only recently [4-6].

The stress analysis of the test is based on the shear-lag theory of Cox [7], as modified by Greszczuk [8] and Lawrence [9] for elastically loaded brittle matrices. A good review of recent developments in this area is given by Gray [10]. In the absence of a chemical bond across the interface, or if an existing bond is broken, the resistance to fiber pull-out is mainly from interfacial frictional stresses, τ. If the matrix shrinks more than the fiber (due to thermal expansion), a residual compressive stress acting at the interface is produced, which depends on the elastic properties of the fiber and matrix, the difference in thermal expansion between the fiber and matrix, and the temperature difference between the glass strain point (T_s) and room temperature (T_{rt}). When $\alpha_{glass} > \alpha_{SiC}$, a larger thermal expansion coefficient difference should lead to a larger compressive stress, and thus to a higher resistance to pull-out. To confirm this hypothesis, experimental data were collected on a soda-lime-silica glass/SiC fiber system for comparison with data [4] on a borosilicate glass/SiC fiber system.

BACKGROUND

In a previous study [4] of a borosilicate glass/SiC monofilament system, a simple model was used where τ was estimated as the maximum pull-out force divided by the contact area. The contact area was taken to be $2\pi rL$, where r is the fiber radius and L is the initial embedded length. This value of τ is probably related to the debonding of the fiber from the matrix. This model is inaccurate since it does not account for Poisson contraction of the fiber radius as a result of the tensile pull-out force nor does it account for shear

Mat. Res. Soc. Symp. Proc. Vol. 120. © 1988 Materials Research Society

stresses occurring where the fiber emerges from between the glass plates. This latter effect is assumed to be a fixed quantity which cannot yet be accounted for. In the present paper, we have used the model of Takaku and Arridge [11], which takes into account the effect of Poisson's contraction. Their expression for the axial stress acting on the fiber is:

$$\sigma_f = \sigma_0/k\ [1 - \exp(-2\mu kL/r)] \qquad (1)$$

where σ_0 is the normal compressive stress acting at the interface in the unstressed material, k is a constant determined by the elastic properties of the fiber and matrix [$= E_m \nu_f / E_f(1+\nu_m)$; E is Young's modulus, ν is Poisson's ratio], and μ is the friction coefficient. By measuring σ_f as a function of embedded length, in principle we can obtain values for σ_0 and μ. As demonstrated in reference 4, however, due to scatter in the data for σ_f, a reliable value for σ_0 could not be obtained in this way. We therefore determined σ_0 using the expression of Vedula et. al. [12] for the residual stress developed in a composite due to anisotropic thermal expansion of fiber and matrix:

$$\sigma_0 \equiv \sigma_{rf} = (\sigma_1\ \Delta\alpha_l + \sigma_2\ \Delta\alpha_r)\ \Delta T \qquad (2)$$

where σ_1 and σ_2 are constants, $\Delta\alpha_l$ and $\Delta\alpha_r$ are the differences in thermal expansion coefficients between the fiber and matrix in the longitudinal and radial directions respectively, and ΔT is the cooling range viz. T_{rt}-T_s.

EXPERIMENTAL PROCEDURE

Soda-lime-silica glass has a thermal expansion coefficient of 82 x 10^{-7}/°C compared to 32 x 10^{-7}/°C for borosilicate glass. The SiC monofilament longitudinal expansion is 26 x 10^{-7}/°C, while the radial expansion is 25.3 x 10^{-7}/°C [6]. Samples were fabricated by sandwiching SiC monofilaments* between soda-lime-silica glass plates* and heating under dead weight loading corresponding to 14-21 KPa pressure as shown in Figure 1. Molybdenum sheets were placed between the dead weight and the glass plates to prevent adhesion during fabrication. The entire assembly was immersed in graphite powder to prevent oxidation of the fibers. Industrial grade argon was kept flowing through the furnace. The samples were held at temperature (725-760°C) for different times (30-90 min) to obtain good flow of the glass around the monofilament. A schematic of the finished samples is shown in Figure 1. Different embedded lengths were obtained by varying the length of the monofilament between the plates. Individual samples were loaded in uniaxial tension on a universal test machine#. The samples were gripped using swivel hooks attached to ball joints to facilitate alignment of the fiber with the stress axis. Samples were pulled at a rate of 0.05 cm/min. The embedded length was determined from the force-displacement curves (Figure 2) since accurate optical measurements could not be made due to uncertainty in where the monofilament emerged from between the glass plates.

---

* SCS-6 SiC monofilaments, AVCO Corp., Lowell, MA. Trade names and companies are identified in order to adequately specify the materials used. In no case does such identification imply that the products are necessarily the best available for the purpose.

* Fisher Brand, Fisher Scientific, Pittsburgh, PA.

Instron Corp., Canton, MA.

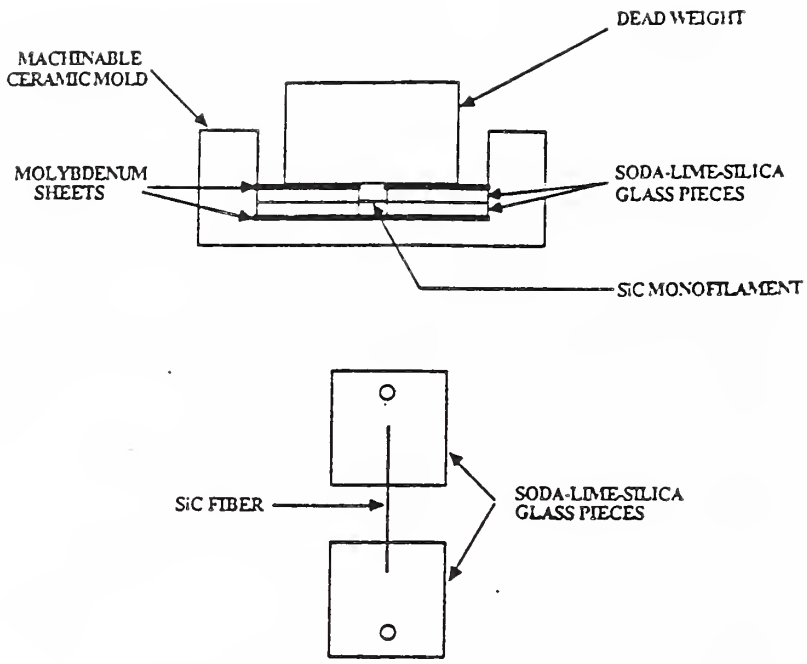

Figure 1. Schematic of the sample-making mold assembly and individual sample.

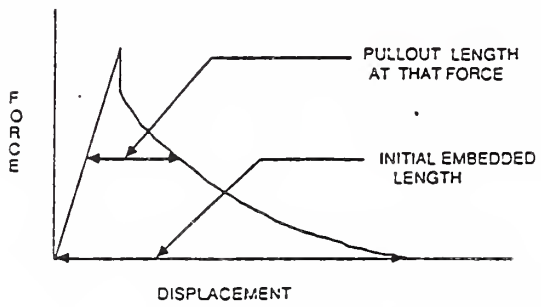

Figure 2. Measurement of pull-out and initial embedded length from a force-displacement curve.

RESULTS AND DISCUSSION

Two types of force-displacement curve were observed in the soda-lime-silica glass/SiC fiber system as shown in Figure 3. In both cases, the load increased linearly with displacement until the fiber debonded from the matrix. In the first case, there was a sharp drop in load, followed by pull-out of the fiber. In the second case, the load decreased gradually from the maximum while the fiber pulled out. The incidence of "stick-slip" behavior during pull-out was much less frequent than in the borosilicate glass/SiC system [4], suggesting the presence of a lubricating layer between the fiber and the soda-lime-silica matrix.

The maximum force required to initiate pull-out of the fiber is plotted vs embedded length in Figure 4. Although there is considerable scatter in the data, it can be seen that the pull-out force increases with increasing embedded length as long as the fiber strength is not exceeded. Some of the scatter may be due to non-uniform flow of glass around the fiber, leading to an air gap at the interface, and therefore reduced contact area and pull-out force. Also plotted in Figure 4 are the loads at which only frictional forces are acting on the interface. The difference between the maximum load and the frictional load is not constant. To confirm that the first load drop is due to debonding, several samples were unloaded following the initial load drop, then reloaded. Upon reloading, pull-out was observed at the same load where unloading had occurred, showing that the fiber-matrix bonds were in fact broken initially and that only frictional stress was operating at the interface. Occasionally, after reloading, a very small load drop was observed which is attributable to the difference between the static and dynamic coefficients of friction. The stability of τ during pull-out over a wide range of instantaneous embedded length is demonstrated in Figure 5.

Table 1 shows τ calculated from Equation 1 for both the soda-lime-silica and borosilicate glass systems. The large standard deviation for the soda-lime-silica system is believed to be due to variations in processing conditions. After making appropriate substitutions in Equation 2 for $\Delta\alpha_f$, $\Delta\alpha_r$, ΔT, σ_1, and σ_2 (see Table 1), the frictional stress, σ_0, for the soda-lime-silica/SiC system is estimated to be about 150 MPa. Similar calculations for borosilicate glass/SiC give a value for σ_0 of about 16 MPa. By substituting values for σ_0 in Equation 1, the friction coefficient, μ, can be obtained. For the soda-lime-silica system, μ was calculated to be 0.10 ± 0.03; for the borosilicate system, μ is 0.72 ± 0.36. The frictional stress acting at the interface may now be calculated as the product of μ and σ_n, where $\sigma_n = \sigma_0 - k\sigma_z$, σ_z being the axial stress corresponding to the frictional force and $k\sigma_z$ representing the reduction in σ_n due to Poisson's contraction. For the soda-lime-silica system, τ was calculated to range from 4-20 MPa while for the borosilicate system, it was in the range from 2-3 MPa.

SUMMARY

(1) Single fiber pull-out tests were used successfully to evaluate the frictional shear stress in glass matrix composites.

(2) For soda-lime-silica glass/SiC monofilament, τ of 4-20 MPa and μ of 0.10 ± 0.03 were obtained. These values may be significantly affected by the glass/fiber/air surface stress discontinuity.

(3) Compared to borosilicate glass system, the frictional stresses in the soda-lime-silica system are higher due to the higher normal compressive stress at the fiber-matrix interface. These higher stresses are the result of the larger difference in thermal expansion coefficients between the soda-lime-silica glass and SiC fiber than between the borosilicate glass and SiC fiber.

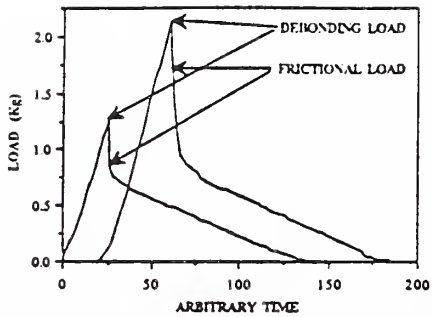

Figure 3. Typical force-time curves observed in soda-lime-silica/SCS-6 system.

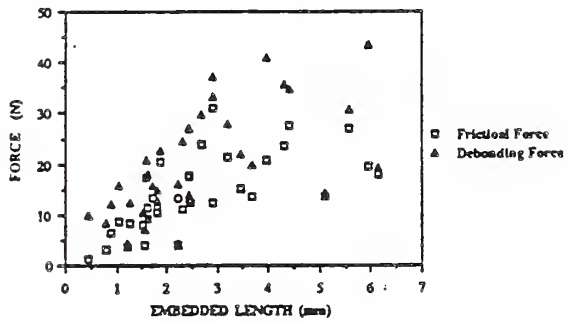

Figure 4. Plot of maximum pull-out force vs embedded length for soda-lime-silica glass/SiC monofilament. Debond force is based on the maximum load observed during the test; frictional force is based on a lower load for which only frictional forces are operating on the interface.

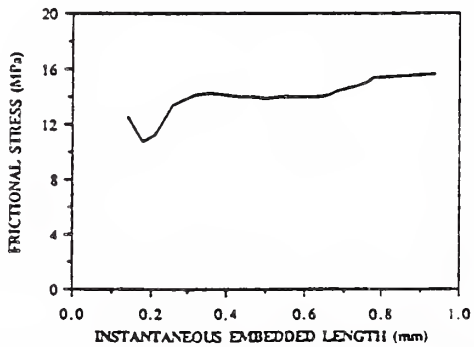

Figure 5. Plot of frictional stress throughout a single pull-out test as a function of instantaneous embedded length.

Table 1
Frictional Shear Stress and Friction Coefficients
Calculated from Equation 1
(Numbers in parenthesis represent number of samples averaged)

Matrix Material	Borosilicate Glass	Soda-Lime-Silica Glass
$\Delta\alpha_f$ (x 10^6/°C)	0.6	5.6
$\Delta\alpha_r$ (x 10^6/°C)	0.67	5.67
ΔT (°C)	495	440
σ_1 (GPa)	6.6	7.5
σ_2 (GPa)	47.0	52.7
σ_0 (MPa)	16.2	153.8
μ	0.72 ± 0.36 (9).	0.10 ± 0.03 (27)
τ (MPa)	3.6 ± 0.7 (9)	13.9 ± 4.1 (27)

(4) The low friction coefficients obtained in the soda-lime-silica system suggest the presence of a lubricating layer between the fiber and the matrix, perhaps due to processing.

ACKNOWLEDGEMENTS

The authors would like to thank Profs. M. J. Koczak and M. Barsoum for helpful discussions. We are grateful to Dr. S. G. Fishman for support through SDIO/IST contract N00014-86-F-0096.

REFERENCES

1) B. Harris, J. Morley, and D. C. Philips, J. Mat. Sci., 10 2050 (1975).

2) M. R. Piggott, A. Sanadi, P. S. Chua, and D. Andison in Composite Interfaces, H. Ishida and J. L. Koenig, Elsevier, 1986, p. 109.

3) L. S. Penn and S. M. Lee, Fibre Sci. Tech., 17 19 (1982).

4) U. V. Deshmukh and T. W. Coyle, to be published in Cer. Eng. Sci. Proc.

5) C. W. Griffin, S. Y. Limaye, D. W. Richerson, and D. K. Shetty, ibid.

6) R. W. Goettler and K. T. Faber, ibid.

7) H. L. Cox, Brit. J. Appl. Phys., 3 72 (1952).

8) L. B. Greszczuk in Interfaces in Composites, ASTM STP 452, 1969, p. 43.

9) P. Lawrence, J. Mat. Sci., 7 1 (1972).

10) R. J. Gray, J. Mat. Sci., 19 861 (1984).

11) A. Takaku and R. G. C. Arridge, J. Phys. D, 6 2038 (1973).

12) M. Vedula, R. N. Pangborn, and R. A. Queeney, Composites, 19 55 (1988).

Ceram. Eng. Sci. Proc., 9 [9-10] pp. 1121-1124 (1988)

A Perspective on Fiber Coating Technology

DAVID C. CRANMER

Ceramics Division
National Bureau of Standards
Gaithersburg, MD 20899

A variety of techniques exist for depositing coatings on ceramic and carbon fibers. This paper reviews several of these techniques and their advantages and disadvantages and points out several deficiencies in uniformly and reproducibly coating the fibers.

Introduction

In examining the key issues involved in developing high quality, tough ceramic matrix composites, one of the most important involves the chemistry and properties of the fiber-matrix interface. Determining appropriate interface composition and properties requires knowledge of the thermodynamics and kinetics of the overall composite (fiber-interface-matrix) system.[1,2] Once an appropriate composition has been determined, appropriate toughening mechanisms can be explored.[3-5] Both carbon and BN surfaces on SiC fibers have been shown to provide toughening behavior in some cases,[1-5] but it is unlikely that either is appropriate for extended use (> 10 hrs) at elevated temperatures (> 1000 °C) in an oxidizing environment.

The fiber-matrix interfacial region can be modified in several ways,[3-6] but because of their versatility, only coating techniques will be considered for interface control. Many techniques exist for putting coatings on ceramic, carbon, and metal substrates. These methods have been reviewed in detail,[7] but when fibers are the substrate, most of the more common methods cannot be used. The basic problem is that many coating methods rely on a line-of-sight between the source material and the substrate, which is not possible for uniformly coating fibers and fiber tows. Given the difficulties inherent in line-of-sight techniques, they will not be discussed further.

The most commonly used techniques for coating fibers are chemical vapor deposition (CVD), metal-organic precursor deposition, and polymer precursor deposition.[8,9] Additional techniques such as electroless plating[10] and eletrodeposition[11] can also be used. Each technique has distinct advantages and disadvantages, which will be discussed below.

Chemical Vapor Deposition

CVD is a vapor transport technique wherein a chemical reaction occurs and the product is deposited on a substrate. There are three types of deposition, two limited by gas diffusion (either of reactants in or products out) and one limited by the reaction rate of the gases to form the deposit. The dominant process is determined by the partial pressure of the reactants and gaseous products, the chemical reactions, and the temperature of the reactor. For coatings, it is preferable to be gas-diffusion limited rather than reaction-rate limited. If the gases react to form the product before reaching the surface as occurs in the reaction-rate limited regime,

the particles produced may not adhere to the fiber or may clump on the surface.

CVD is the most common method currently used for producing coatings on fibers. It uses a fairly simple apparatus (Fig. 1) but requires cleaning of the exhaust gases. A large number of compositions can be deposited with this technique.[12] The coating thickness can range from nanometers to several micrometers, depending on the length of the furnace and/or the number of CVD cycles to which the fibers are exposed. A distinct advantage of the technology is that the fiber coatings can be deposited on a continuous basis, allowing it to be combined with other composite fabrication techniques such as filament winding.

The uniformity of the coating is determined by the ability of the reactant gases to reach the fiber surfaces and the temperature at which the reaction is gas-diffusion limited. The CVD process is a slow one, but methods such as multiple cyclings of the fiber through the deposition chamber can be envisioned which may speed the overall coating process.

Metal-Organic Precursor

The metal-organic precursor (or sol-gel) process typically uses an alkoxide or mixture of alkoxides dissolved in a solvent which coats the fibers and then is made to undergo a chemical reaction to form the final product. The basic technique (Fig. 2) involves drawing the fiber or tow through a bath of the appropriate alkoxide(s), followed by hydrolysis or ammonialysis of the solution to convert the alkoxide to the oxide or nitride, followed by higher temperature treatments to pyrolyze/vaporize any remaining organic materials. Most of the coatings which have been produced to date are simple oxides.

Experience with this technique has shown that single layers of about 150 nm can be produced repeatedly.[13-15] The compositional limits imposed on this process come from the available starting chemicals and the reactions to form the products. The chemistry of these systems can be straightforward as in the case of SiO_2 where

$$Si(OC_2H_5)_4 + 2H_2O - \Delta - SiO_2 + 4C_2H_5OH\ (g) \quad (1)$$

and

$$Si(OC_2H_5)4 - heat - SiO_2 + 2C_2H_5OH\ (g) + 2C_2H_4\ (g) \quad (2)$$

In more complicated multicomponent systems, different constituents may react or precipitate at different times, leading to inhomogeneities in composition or nonuniform thickness.

For thicker coatings (>200 nm), multiple dippings of the fibers are required.[14] While this is a disadvantage for coatings of the same composition, it is very easy to obtain a graded composition coating using this technique. Like the CVD process, this technique can be used to continuously apply the coating to the fibers.

Polymer Precursors

In concept, this technique is almost identical to the metal-organic precursor technique described above. The difference is that a polymer or oligoimer in an appropriate solvent is used (not an alkoxide), and the coated fiber is pyrolyzed to form the ceramic. The apparatus is virtually identical to that shown in Fig. 2 except that the hydrolyzing furnace is removed from the system. The coating composition depends on the specific polymer precursor. This technique has been used to make carbon coatings from pitch precursors[15] and SiC coatings from polycarbosilane.[9] Other coatings which can be made by this technique will depend on the

availability of polymer precursors.[15,16] This method also lends itself to being a continuous process.

Electroless Plating and Electrodeposition

Electroless plating[10] and electrodeposition[11] provide methods for applying metallic coatings. They require a conductive fiber surface for deposition to take place, which can be achieved for some fibers but not for most of those available. They are relatively slow processes and require some clever engineering to make into continuous processes due to the need of a surface charge. Done properly, they provide a uniform coating of metal but their utility for coating multifilament tows is unclear since the effects of interacting surface charges are not known at this point.

Summary

The descriptions and discussions given above show that each of the coating techniques can be used to provide useful materials within certain limits. Almost any desired composition can be applied to a useful thickness using one or more of the techniques. What is still required to design coating systems is a better definition of the coating's purpose (diffusion barrier, reaction inhibitor, or something else), knowledge of the thermodynamics/kinetics of the overall system, as well as methods of coating characterization.

References

[1]P. M. Benson, K. E. Spear, and C. G. Pantano, "Interfacial Characterization of Glass Matrix/Nicalon SiC Fiber Composites: A Thermodynamic Approach," presented at the 12th Annual Conference on Composites and Advanced Ceramic Materials, Cocoa Beach, FL 17-20 Jan. 1988.

[2]K. E. Spear, P. M. Benson, and C. G. Pantano, "Thermochemical Modeling for Interface Reactions in Carbon-Fiber Reinforced Glass Matrix Composites," to be published in the Proceedings of the 172nd Meeting of the Electrochemical Society.

[3]J. J. Brennan, "Additional Studies of SiC Fiber Reinforced Glass-Ceramic Matrix Composites," Technical Report, ONR Contract N00014-82-C-0096, 14 Feb., 1983.

[4]J. J. Brennan, "Interfacial Characterization of Glass and Glass-Ceramic Matrix/Nicalon SiC Fiber Composites," in *Tailoring Multiphase and Composite Ceramics*, R. E. Tressler, G. L. Messing, C. G. Pantano, and R. E. Newnham, eds., Plenum Press, New York, 1986, pp. 549-560.

[5]B. Bender, D. Shadwell, C. Bulik, L. Incorvati, and D. Lewis, "Effect of Fiber Coatings and Composite Processing on Properties of Zirconia-Based Matrix SiC Fiber Composites," *Am. Cer. Soc. Bull.*, 65 [2], 363-369 (1986).

[6]K. M. Prewo and J. J. Brennan, "High-Strength Silicon Carbide Fibre-Reinforced Glass-Matrix Composites," *J. Mat. Sci.*, 15 (1980) 463-468.

[7]T. E. Schmid, "High Technology Ceramic Coatings—Current Limitations—Future Needs," presented at the 12th Annual Conference on Composites and Advanced Ceramic Materials, Cocoa Beach, FL, 17-20 Jan. 1988.

[8]R. N. Singh and M. K. Brun, "Effect of Boron Nitride Coating on Fiber-Matrix Interactions," *Cer. Sci. Eng. Proc.*, 8 [7-8], 636-643 (1987).

[9]H. Katzman, "Fiber Wetting and Coatings for Composite Fabrication," SD-TR-86-63, The Aerospace Corporation, Oct. 1986.

[10]L. S. Evans and P. E. Morgan, "Method for Producing a Metal Composite," U. S. Patent 3 550 247, 29 Dec. 1970.

[11]D. S. Lashmore, "Electrodeposition."

[12]*Chemical Vapor Deposition, Second International Conference*, J. M. Blocher, Jr., and J. C. Withers, eds., The Electrochemical Society, New York, 1970, 861 pp.

[13]D. C. Cranmer and D. J. Speece, "Fiber-Matrix Interactions in Carbon Fiber/Cement Matrix Composites," in *Tailoring Multiphase and Composite Ceramics*, R. E. Tressler, G. L. Messing, C. G. Pantano, and R. E. Newnham, eds., Plenum Press, New York, 1986, pp. 609-614.

[14]H. Katzman, "Pyrolyzed Pitch Coatings for Carbon Fiber," U. S. Patent 4 376 804, Mar. 1983.

[15]F. Hurwitz, L. Hyatt, J. Gorecki, and L. D'Amore, "Silsequioxianes as Precursors to Ceramic Composites," *Cer. Sci. Eng. Proc.*, 8 [7-8], 732-743 (1987).

[16]K. J. Wynne and R. W. Rice, "Ceramics via Polymer Pyrolysis," in *Annual Reviews of Materials Science 1984*, Vol. 14, 1984, pp. 297-334.

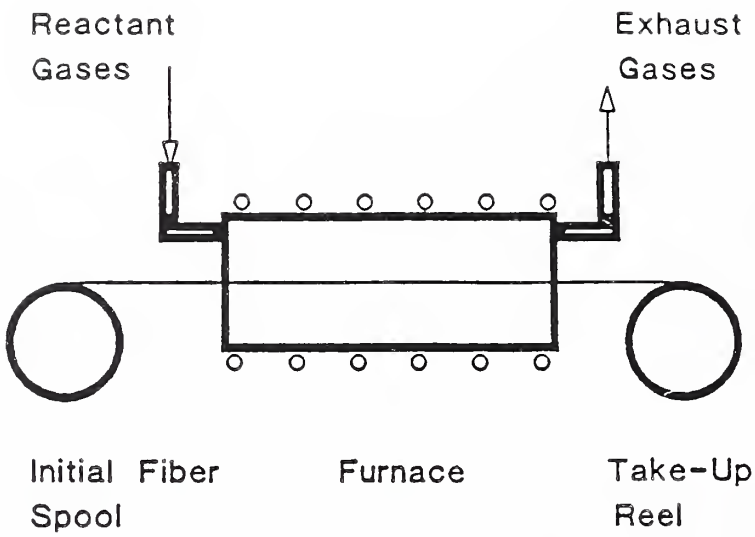

Fig. 1. Schematic of chemical vapor deposition apparatus for fiber coating.

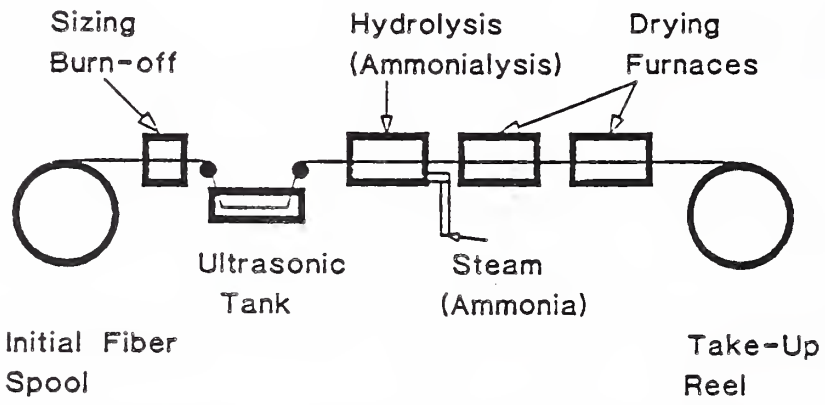

Fig. 2. Schematic of metal-organic precursor apparatus for fiber coating.

To be published in ASTM Special Technical Publication: Symposium on Thermal and Mechanical Properties of Metal and Ceramic Matrix Composites

COMPARISON OF METHODS FOR DETERMINING FIBER/MATRIX INTERFACE FRICTIONAL STRESSES IN CERAMIC MATRIX COMPOSITES

David C. Cranmer*, Uday V. Deshmukh+, and Thomas W. Coyle#

*National Institute of Standards and Technology, Gaithersburg, MD 20899

+Dept. of Materials Engineering, Drexel University, Philadelphia, PA 19104

#Ecole Nationale Superieure de Mechanique, Nantes Cedex, FRANCE

ABSTRACT: In this study, several experimental methods including indentation push-in, indentation push-out, and single fiber pull-out tests were employed to measure the strength of the fiber/matrix bond in two continuous fiber reinforced ceramic matrix composites. The composite systems examined were a SiC monofilament reinforced borosilicate glass matrix and a SiC fiber tow reinforced glass-ceramic matrix. Single fiber pull-out test results gave debond strengths (τ_d) of 11.1 ± 3.2 MPa and interface frictional stresses (τ_f) of 3.6 ± 0.7 MPa for the SiC/borosilicate system. In the push-out test, τ_d for the SiC/borosilicate system appears to be about 10 MPa while τ's between 1 and 55 MPa were obtained in the SiC/glass-ceramic composite. The push-in test gave values of τ_f between 2 and 34 MPa for the SiC/glass-ceramic system. Variability in τ within a specimen is due to differences in bonding between the fibers and matrix at various locations. The discrepancies in τ both within a test and between test methods are explained in terms of fiber/matrix bonding and test geometry. The most versatile test method appears to be the indentation push-out test.

Key Words: glass-ceramic composites, glass composites, mechanical properties, fiber/matrix interfacial strength, indentation push-in, indentation push-out, fiber pull-out

INTRODUCTION

The strength of the fiber-matrix interface is one of the key parameters responsible for the stress-strain behavior and damage tolerance of ceramic composites. These interfacial strengths (τ) have been measured by several different techniques [1-6] including indentation push-in, indentation push-out, and single fiber pull-out. The interfacial strength which can be measured is one of two types: debond (τ_d) and frictional (τ_f). The debond strength is related to the degree of chemical bonding between the fiber and the matrix, while the frictional stress relates to the slippage of the fiber in the matrix. The purpose of this paper is to compare these methods for obtaining τ_d and τ_f, both in terms of the ease of use and the consistency and reproducibility of the numbers obtained from each technique.

As will be shown in more detail in the Background Section, no one material lends itself to testing using all three methods, and no single test method provides all of the information desired on interfacial mechanical properties. The reasons for this are as follows. In a single fiber pull-out test, the combination of a small fiber diameter (10-20 μm) for materials such as Nicalon SiC[1], high temperature (>700°C) processing required to obtain an acceptable sample geometry, and handling to set up each experiment makes it difficult at best to perform the test on a large

---

[1] Nicalon SiC, Nippon Carbon Co., Ltd., Tokyo, Japan. Trade names and companies are identified in order to adequately specify the materials and equipment used. In no case does such identification imply that the products are necessarily the best available for the purpose.

enough number of samples. In the indentation push-in test, the large monofilaments tend to crush rather than slide, thus obliterating the indentation impressions and yielding inaccurate displacement measurements. To date, no work has been published regarding the use of the indentation push-out test on layered fibers such as SiC deposited on C or W cores. In view of these problems, two model composite systems were chosen which were amenable to measurements by more than one technique. The model systems examined include a borosilicate glass matrix reinforced by SiC monofilaments[2] and a lithium aluminosilicate glass-ceramic matrix reinforced by SiC fibers[3]. The borosilicate glass system was tested using the pull-out and indentation push-out techniques, while the glass-ceramic system was tested using the two indentation techniques.

BACKGROUND

Single Fiber Pull-out

Single fiber pull-out tests give the most direct measure of the interface strength [6-11], but the tests performed to date have only been conducted on monofilaments. Depending on the nature of the interaction (chemical and/or mechanical) between the fiber and the matrix, the single fiber pull-out test gives information about both the debonding and frictional processes occurring in composites. However, single fiber pull-out tests have been used for glass matrix systems only recently [6,10,11].

---

[2] SCS-6, Textron Specialty Materials, Lowell, MA.

[3] Nicalon SiC/LAS-III, United Technologies Research Center, East Hartford, CT.

In a previous study [10] of a SiC/borosilicate glass monofilament system, τ_f was determined as 5 - 6.5 MPa. A simple model based on a shear-lag analysis was used where τ was estimated as the pull-out force divided by the contact area. This model is inaccurate since it does not account for differential Poisson contractions of the fiber and matrix as a result of the tensile pull-out force nor does it account for surface stress concentrations occurring where the fiber emerges from between the glass plates. In a subsequent paper [5], Poisson contraction was taken into account, and τ_f was determined to be on the order of 3.5 MPa, a decrease of 30-45% compared to that calculated using the simple analysis. In this same paper, τ_d was determined to be 11 MPa.

An alternate analysis [6], also based on the shear lag theory, yields τ_f's between 15 and 30 MPa, depending on the exact glass composition. This analysis assumes the presence of a residual stress in the fiber due to thermal expansion mismatch between the fiber and the matrix. Evaluation of the interfacial frictional stress is thus broken into two components: one a residual stress-free bonding term (τ_0), the other the contribution due to residual stresses ($\mu\sigma_{rm}$). τ_0 should vary with fiber surface chemistry, while $\mu\sigma_{rm}$ should vary with processing conditions, sample geometry, and matrix composition. The values of τ_f obtained in reference 6 are significantly higher than obtained using the previous analyses. At present, there is insufficient basis, either experimental or theoretical, on which to choose one model over the other.

Indentation Tests

Indentation testing to determine τ_f was first initiated by Marshall [1]. Fiber/matrix frictional stresses of 2.5 ± 0.9 MPa were measured for a

SiC-reinforced glass-ceramic[2], but the method requires precise measurement of very small indentation sizes, potentially a significant source of error. The analysis assumes that the elastic depression of the matrix adjacent to the indented fiber, the stress field of the indent and the surface stress concentrations, as well as changes in fiber diameter due to Poisson's expansion can be neglected. For the analysis to be valid, the specimen thickness must be large compared to the diameter of the fiber. The analysis also does not account for non-orthogonal loading of the fiber or misorientation of the fiber from a direction parallel to the applied force. Additional studies by Marshall and Oliver [3] refined the method by using a pyramidal indenter at ultralow loads (< 0.12 N). In this method, the indenter is instrumented to provide independent determinations of force applied to the fiber and displacement of the fiber in the matrix. The revised method permits examination of both debonding and frictional sliding in a SiC/glass-ceramic composite. Values of τ_f on the order of 3.5 MPa were obtained on this material, in good agreement with the initial measurements using the Vickers diamond. One particular aspect of this method which limits its use is the special apparatus required to apply very small loads, although efforts are currently being made to expand the load range which can be applied [19]. While most of the work on the indentation push-in test has been conducted using a standard Vickers diamond geometry, Mandell et al [2] have shown that the shape of the indenting diamond can be changed to increase the amount of sliding which can be observed.

While the typical indentation push-in test uses the Vickers diamond to push the fiber into the matrix, the indentation push-out test uses the diamond to push the fiber through the matrix. The push-out test requires the use of thinner specimens (< 2-3 mm) than the push-in test. The basic

assumptions in the analysis of the push-out test are the same as for the push-in test and also neglects stress concentrations at the bottom surface where the fiber emerges during the test. In the push-out test, three regimes are envisioned: an initial region in which the diamond is in contact with the fiber only and the sliding length is less than the thickness of the sample, a plateau region in which the sliding length is greater than or equal to the thickness of the sample, and a final region in which the diamond makes contact with and deforms the matrix. These regimes are shown schematically in Figure 1. In principle, the initial regime also represents the behavior of the push-in test; however, the assumption that specimen thickness is much greater than the fiber diameter is not valid if the thickness is too small. In addition, the surface stress concentrations will play a larger role than in thicker samples. In the initial regime, τ is determined from the slope (m) of a plot of the force on the fiber squared (F^2) versus displacement (δ):

$$\tau = m/4\pi^2 R^3 E_f \qquad (1)$$

where R is the radius of the fiber and E_f is the elastic modulus of the fiber. In the plateau region of the curve, τ is determined from the force at which the plateau occurs:

$$\tau = F/2\pi Rt \qquad (2)$$

where t is the thickness of the specimen. In the last regime, where the diamond is in contact with the matrix, τ cannot be determined. Which value of τ (debond or frictional) is measured in the plateau region depends on whether or not there is a chemical bond between the fiber and matrix and what geometry indenter is being used. In the typical geometry using a standard Vickers diamond, when the fiber debonds, the frictional stress is also exceeded and the fiber slips until either contact with the surrounding

matrix occurs or until friction slows the fiber displacement to a value expected from frictional stresses alone. If no debonding must occur, then only slippage due to friction is present.

For large monofilaments such as the SCS-6 SiC, where the SiC is deposited on a carbon core, two plateaus are expected. The first occurs when the carbon core (33 μm diameter) slips in the SiC; the second when the SiC fiber (about 140 μm diameter) slips in the matrix. The fiber displacements at which each of these events takes place can be calculated from the geometry of the Vickers diamond. The diamond should make contact with the SiC at a displacement of about 5 μm, and it should contact the matrix at a displacement of 20 μm. Thus a plateau occuring prior to 5 μm can be attributed to the slippage of the carbon core, and one occuring prior to 20 μm can be attributed to slippage of the SiC. Whether one plateau or two plateaus occur depends on the debond strength of the interfaces between the core and SiC, and between the SiC and the surrounding matrix.

EXPERIMENTAL PROCEDURE

Single fiber pull-out samples were fabricated by sandwiching SiC monofilaments between borosilicate glass plates and heating under dead weight loading corresponding to 14-21 KPa pressure. Molybdenum sheets were placed between the dead weight and the glass plates to prevent adhesion during fabrication. The entire assembly was immersed in graphite powder to prevent oxidation of the fibers. Industrial grade argon was kept flowing through the furnace. The samples were held at 760°C for 60 min to obtain good flow of the glass around the monofilament. A schematic of the finished samples is shown in Figure 2. Different embedded lengths were

obtained by varying the length of the monofilament between the plates. Individual samples were loaded in uniaxial tension on a screw-driven universal test machine[4]. The samples were gripped using swivel hooks attached to ball joints to facilitate alignment of the fiber with the stress axis. Samples were pulled at a rate of 0.05 cm/min. The embedded length was determined from the force-displacement curves (Figure 3), since accurate optical measurements prior to testing could not be made due to uncertainty in where the monofilament emerged from between the glass plates.

The materials for the indentation tests were either obtained from commercial sources (glass-ceramic, see footnote 2) or made by hot pressing a sample of SiC/borosilicate glass at 800°C for 30 minutes at about 14 KPa. The indentation tests were performed using an instrumented indenter, allowing for independent determinations of force and displacement. A schematic of the test apparatus is shown in Figure 4. Displacement was determined using a pair of capacitance probes; the change in capacitance in a probe varies as it approaches a fixed target. Targets were fixed with respect to the specimen surface, and each probe was initially calibrated using a laser interferometer. Specimens for indentation included 1 mm and 2 mm thick multifilament SiC/glass-ceramic and 0.3 mm thick monofilament SiC/borosilicate glass. The samples were at least partially flat and polished so that the capacitance probes did not have to be adjusted frequently. A 50 g load was used for the SiC/glass-ceramic material, and the loads ranged from 130 to 150 g for the SiC/borosilicate material. Based on the debond strength of the SiC/glass, as determined from the single fiber pull-out test (9 MPa), loads < 140 g should exhibit a single

[4] Instron Corp., Canton, MA.

plateau of the core slipping in the SiC while loads > 140 g should exhibit both plateaus.

RESULTS AND DISCUSSION

As noted above, which value of τ is measured depends on the test method employed as well as the material being tested. It is expected that the single fiber pull-out test will provide information on both debonding strength and frictional stresses, while the push-in test will measure frictional stresses only. The push-out test could measure either or both debond strength or frictional stress, depending on the material and the indenter geometry.

Two types of force-displacement curve were observed in the SiC monofilament/borosilicate glass system as shown in Figure 5. In both cases, the load increased linearly with displacement until the fiber debonded from the matrix. In the first case, there was a sharp drop in load, followed by pull-out of the fiber. In the second case, the load decreased gradually from the maximum while the fiber pulled out. The two types of curves may indicate two types of interface failure. A sudden drop indicates catastrophic failure of the entire interface whereas the smoother curve indicates a more gradual, incremental failure of the interface.

The maximum force required to initiate pull-out of the fiber vs embedded length is plotted in Figure 6. Although there is considerable scatter in the data, it can be seen that the pull-out force increases with increasing embedded length as long as the fiber strength is not exceeded. Some of the scatter may be due to non-uniform flow of glass around the fiber during hot pressing, leading to an air gap at the interface, and therefore reduced contact area and pull-out force. Also plotted in Figure

6 are the loads at which only frictional forces are acting on the interface. The difference between the maximum load and the frictional load is not constant. To confirm that the first load drop is due to debonding, several samples were unloaded following the initial load drop, then reloaded. Upon reloading, pull-out was observed at the same load where unloading had occurred, showing that the fiber-matrix bonds were in fact broken initially and that only frictional stresses were operating at the interface. Occasionally, after reloading, a very small load drop was observed which is attributable to the difference between the static and dynamic coefficients of friction. The stability of τ during pull-out over a wide range of instantaneous embedded length is demonstrated in Figure 7.

The values of τ_f measured using the single fiber pull-out test for the SiC/borosilicate system are lower than those obtained by Goettler and Faber [6] (12.5 MPa), but, as noted in the Background Section, the analytical methods were different, as were the specimen fabrication procedures. When the data of Deshmukh and Coyle [4] for SiC reinforced borosilicate glass are examined using the analysis of Equation 4, a value of τ_f of 22 MPa is obtained. When the expected residual stresses are taken into account (Equations 5a and 5b), a value of τ_0 between 7 and 18 MPa is found, depending on the choice of friction coeffient (0.2 vs 0.72). A friction coefficient of 0.72 is the value taken from reference 4, while $\mu = 0.2$ is that determined in reference 6. Both values of τ_0 are in good agreement with the result of Goettler and Faber for the same nominal composition matrix.

For the SiC/borosilicate glass system, the push-out test shows either one or two plateaus (Figure 8). As described above, based on the debond strength of SiC/glass, loads < 140 g should exhibit a single plateau while

those > 140 g should exhibit two plateaus. The first case is shown in Figure 8a. The force at the plateau gives a value of τ_d of 38 MPa for the core slipping through the SiC. The second case is shown in Figure 8b, where the force at the first plateau gives a value of τ of 36 MPa for the core slipping in SiC and the force at the second plateau gives a value of τ of 10 MPa for the SiC slipping in the matrix. Tests on additional fibers gave an average value of τ of 30 ± 9 MPa for the core in SiC. The value of τ for SiC in the matrix is in reasonable agreement with τ_d obtained from the single fiber pull-out test. These results are based on a fairly small number of fibers and additional verification is required to more firmly establish these values. In addition to more data, precise measurements of the indentations need to be made and Marshall's analysis applied to the data to confirm that the two methods agree. Examination of the SiC/glass-ceramic system shows that τ is dependent on the investigator as well as the technique. The indentation push-in results yield τ's varying from 1 to 10 MPa, depending on the investigator [1,3-5,10] and from 1 to 100 MPa, depending on the heat treatment [4]. The discrepancy in heat treated materials is due to differences in the fiber-matrix interface bonding with some fibers being more tightly bound than others. This would lead to differences in both debond strength and frictional pull-out. The discrepancy in various untreated materials is due to both differences in the fiber-matrix bond and fiber misorientation with respect to the applied force. In a sample which is 2 mm in thickness, the indentation test was either of the push-in or push-out type. Typical results are shown in Figure 9. In Figure 9a, a push-in type is shown while Figure 9b shows a push-out result. In both cases, however, τ is on the order of 1-6 MPa for this system, leading to the conclusion that this τ is due to frictional

effects. Values of τ as high as 55 MPa were also observed, leading to the supposition that there are differences in the bonding between fiber and matrix at different locations in the specimen. The indentation push-out test results are more difficult to obtain because of the need to use flat and polished samples. Based on a number of measurements, however, the indentation push-out results are more reproducible than are the indentation push-in results. For this thickness sample, it is apparent that the assumptions for both types of test are met. For thinner samples, the assumption that the thickness >> fiber diameter may be violated, thus τ_f determined from the plateau region of the push-out test may not agree with that obtained in the initial region where push-in is assumed to take place. The analysis of the push-out test in the plateau region is simpler than that required for the push-in test and is not affected by the assumptions regarding elastic interactions after the force is released and what happens below the slip region during testing.

CONCLUSIONS

Each of the test methods discussed in this paper has advantages and disadvantages. The single fiber pull-out test provides the most direct method of determining the interfacial strengths, both debonding and frictional, but at present can only be used effectively for large fiber diameters, primarily due to specimen handling considerations. The indentation tests use a minimal amount of material and can be performed on samples containing either large monofilaments or small diameter multifilament tows but provide information on only τ_f (push-in) or τ_f or τ_d (push-out), depending on indenter geometry and material characteristics. It is possible that the push-out test can be performed at slower loading

rates and with a different indenter geometry, thus allowing for separation of the debonding strength from the interfacial friction stress in the force^2-displacement curve. The preparation of indentation push-out samples is more difficult than for indentation push-in samples but the analysis is simpler and the results appear to be more reproducible. While there are some discrepancies yet to be resolved, interfacial strengths determined using different test methods agree well with one another as do debond strengths determined using different methods.

Based on the ability to measure both debond strength and interfacial frictional stress, and the need to use a minimal amount of material, the indentation push-out test appears to be the most desirable one to use.

ACKNOWLEDGEMENTS

The authors would like to thank S. W. Freiman, E. R. Fuller, Jr., M. J. Koczak, and M. Barsoum for many helpful discussions. We are grateful to Dr. S. G. Fishman for support through SDIO/IST contract N00014-86-F-0096.

REFERENCES

1) Marshall, D. B., Journal of the American Ceramic Society, Volume 66, December, 1984, pp. C259-C260.

2) Mandell, J. F., Grande, D. H., Tsiang, T.-H., and McGarry, F. J., in Composite Materials: Testing and Design, ASTM STP 893, J. M. Whitney, ed., ASTM, Philadelphia, 1986, pp. 87-108.

3) Marshall, D. B., and Oliver, W. C., Journal of the American Ceramic Society, Volume 70, August, 1987, pp. 542-548.

4) Coyle, T. W., Chan, H. M., and Deshmukh, U. V., in Interfaces in Polymer, Ceramic, and Metal Matrix Composites, H. Ishida, ed., Elsevier, Amsterdam, 1988, pp. 489-501.

5) Deshmukh, U. V., Kanei, A., Freiman, S. W., and Cranmer, D. C., in High Temperature/High Performance Composites, MRS Symposium Volume 120, Materials Research Society, 1988.

6) Goettler, R. W., and Faber, K. T., Ceramic Engineering and Science Proceedings, Volume 9, 1988, pp. 861-870.

7) Harris, B., Morley, J., and Philips, D. C., Journal of Material Science, Volume 10, 1975, pp. 2050-2061.

8) Piggott, M. R., Sanadi, A., Chua, P. S., and Andison, D. in Composite Interfaces, H. Ishida and J. L. Koenig, Eds., Elsevier, Amsterdam, 1986, pp. 109-121.

9) Penn, L. S., and Lee, S. M., Fibre Science and Technology, Volume 17, 1982, pp. 91-97.

10) Deshmukh, U. V., and Coyle, T. W., Ceramic Engineering and Science Proceedings, Volume 9, 1988, pp. 627-634.

11) Griffin, C. W., Limaye, S. Y., Richerson, D. W., and Shetty, D. K., Ceramic Engineering and Science Proceedings, Volume 9, 1988, pp. 671-678.

12) Cox, H. L., British Journal of Applied Physics, Volume 3, March 1952, pp. 72-79.

13) Greszczuk, L. B., in Interfaces in Composites, ASTM STP 452, 1969, pp. 43-58.

14) Lawrence, P., Journal of Materials Science, Volume 7, 1972, pp. 1-6.

15) Gray, R. J., Journal of Materials Science, Volume 19, 1984, pp. 861-870.

16) Takaku, A., and Arridge, R. G. C., Journal of Physics D: Applied Physics, Volume 6, 1973, pp. 2038-2047.

17) Vedula, M., Pangborn, R. N., and Queeney, R. A., Composites, Volume 19, January, 1988, pp. 55-60.

18) Oel, H. J., and Frechette, V. D., Journal of the American Ceramic Society, Volume 69, April, 1986, pp. 342-346.

19) Lowden, R. A., Oak Ridge National Laboratory, private communication, 1988.

Table 1

Frictional Shear Stress for Two Composite Systems

τ_f in MPa

(Numbers in parenthesis represent number of samples averaged)

Technique	Reference	Nicalon/LAS III	SCS-6/Borosilicate
Single Fiber Pull-Out			
Poisson's Contraction	5	-	3.6 ± 0.7 (9)
Residual Stress	6	-	15 - 28
Residual Stress-Free	6	-	12.5
Simple Analysis	10	-	5 - 6.5
Simple Analysis	This study	-	5.6 ± 2.7 (8)
Indentation Push-In			
Vickers Diamond	1	2.5 ± 0.9 (10)	-
Nanoindenter	3	3.5	-
Rapid Loading	3	2.1 ± 1.5 (70)	-
Vickers Diamond	4	1 - 100	-
Instrumented Indenter	This study	1 - 55	-
Indentation Push-Out			
Instrumented Indenter	This study	2 - 34	9 - 10

Figure Captions

Figure 1. Schematic of force squared/displacement for indentation push-out test

Figure 2. Schematic of the sample-making mold assembly and individual sample.

Figure 3. Measurement of pull-out and initial embedded length from a force-displacement curve.

Figure 4. Schematic of indentation apparatus.

Figure 5. Typical force-time curves observed in SiC monofilament/borosilicate system.

Figure 6. Plot of maximum pull-out force vs embedded length for SiC monofilament/borosilicate glass. Debond force is based on the maximum load observed during the test; frictional force is based on a lower load for which only frictional forces are operating on the interface.

Figure 7. Plot of frictional stress throughout a single pull-out test as a function of instantaneous embedded length.

Figure 8. Results of indentation of SiC monofilament in borosilicate glass matrix.
a. Indentation load = 130 grams.
b. Indentation load = 150 grams.

Figure 9. Results of indentation of SiC in lithium aluminosilicate matrix.
a. Push-in result ($l < t$)
b. Push-out result ($l > t$)

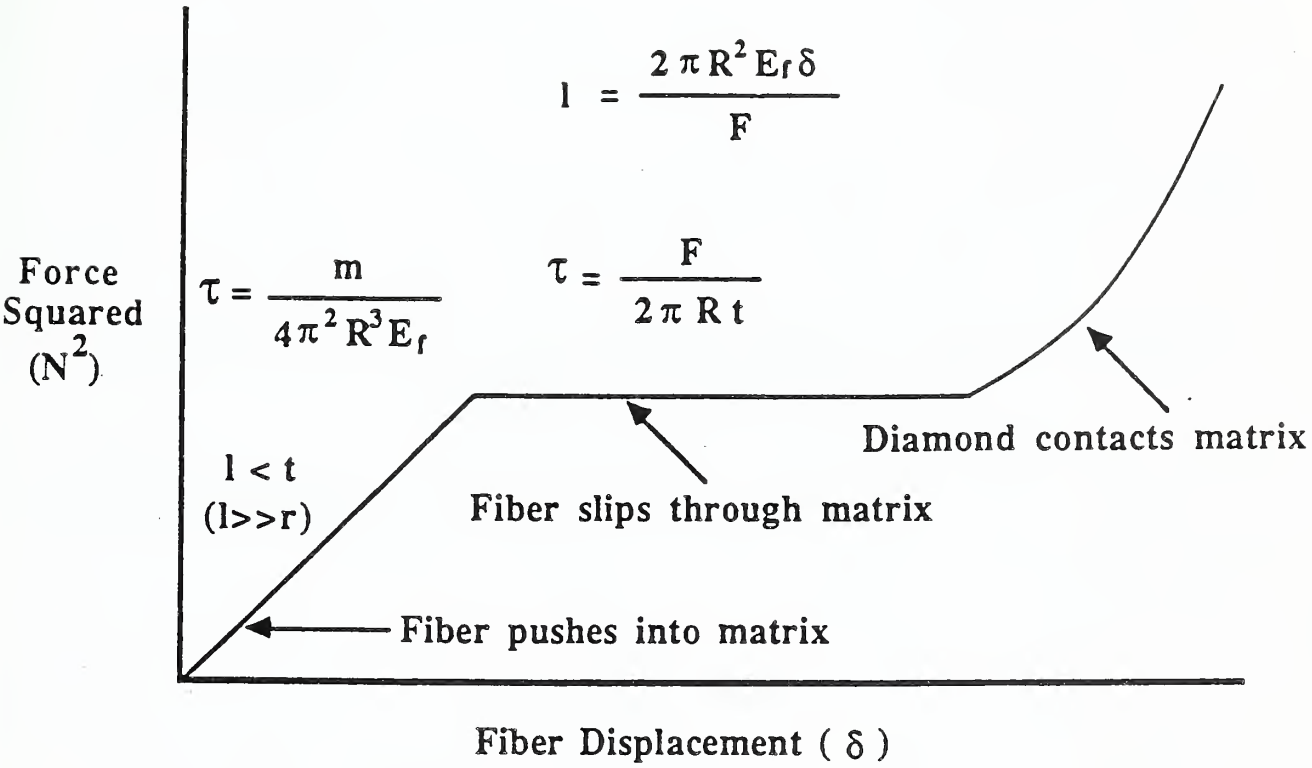
$l = \frac{2\pi R^2 E_f \delta}{F}$
Force Squared (N^2)
$\tau = \frac{m}{4\pi^2 R^3 E_f}$
$\tau = \frac{F}{2\pi R t}$
$l < t$
$(l >> r)$
Diamond contacts matrix
Fiber slips through matrix
Fiber pushes into matrix
Fiber Displacement (δ)

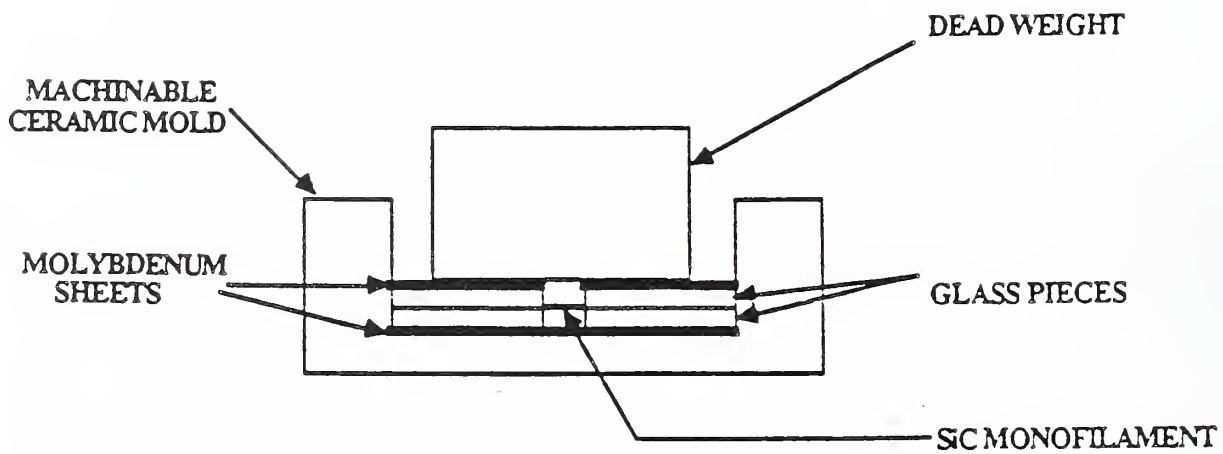
DEAD WEIGHT
MACHINABLE
CERAMIC MOLD
MOLYBDENUM
SHEETS
GLASS PIECES
SiC MONOFILAMENT

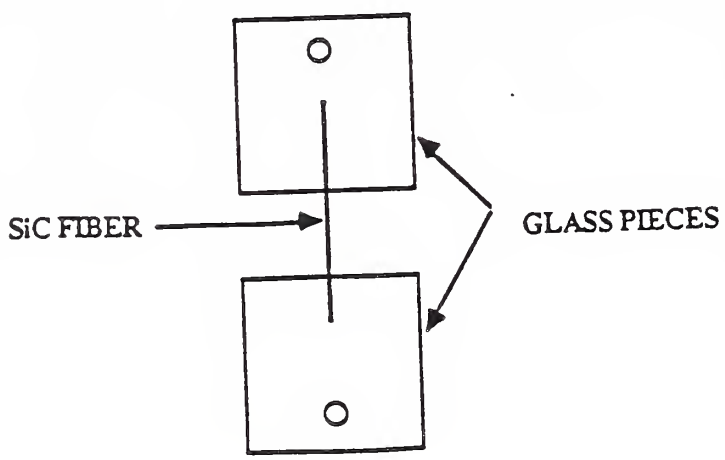
SiC FIBER
GLASS PIECES

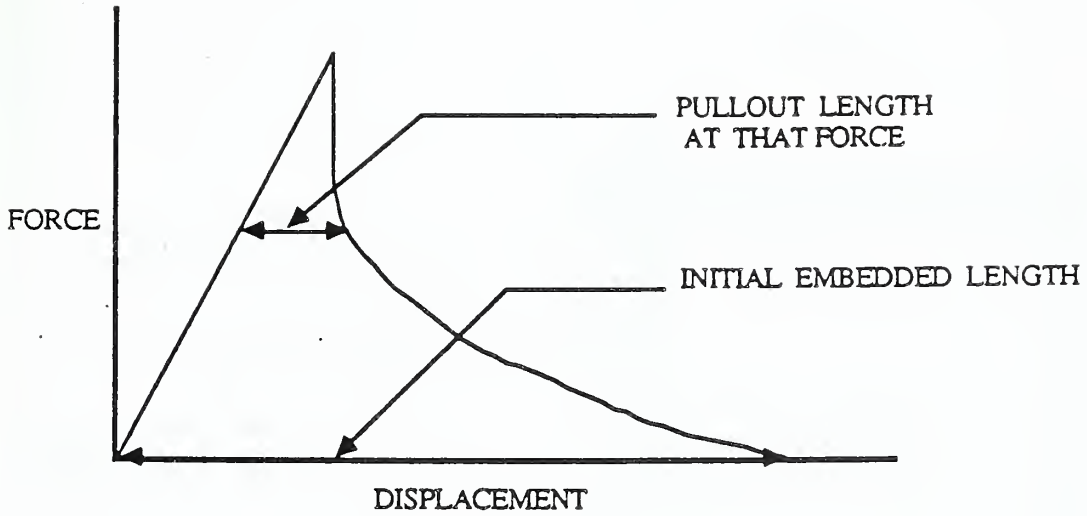
PULLOUT LENGTH
AT THAT FORCE
FORCE
INITIAL EMBEDDED LENGTH
DISPLACEMENT

Figure 3.

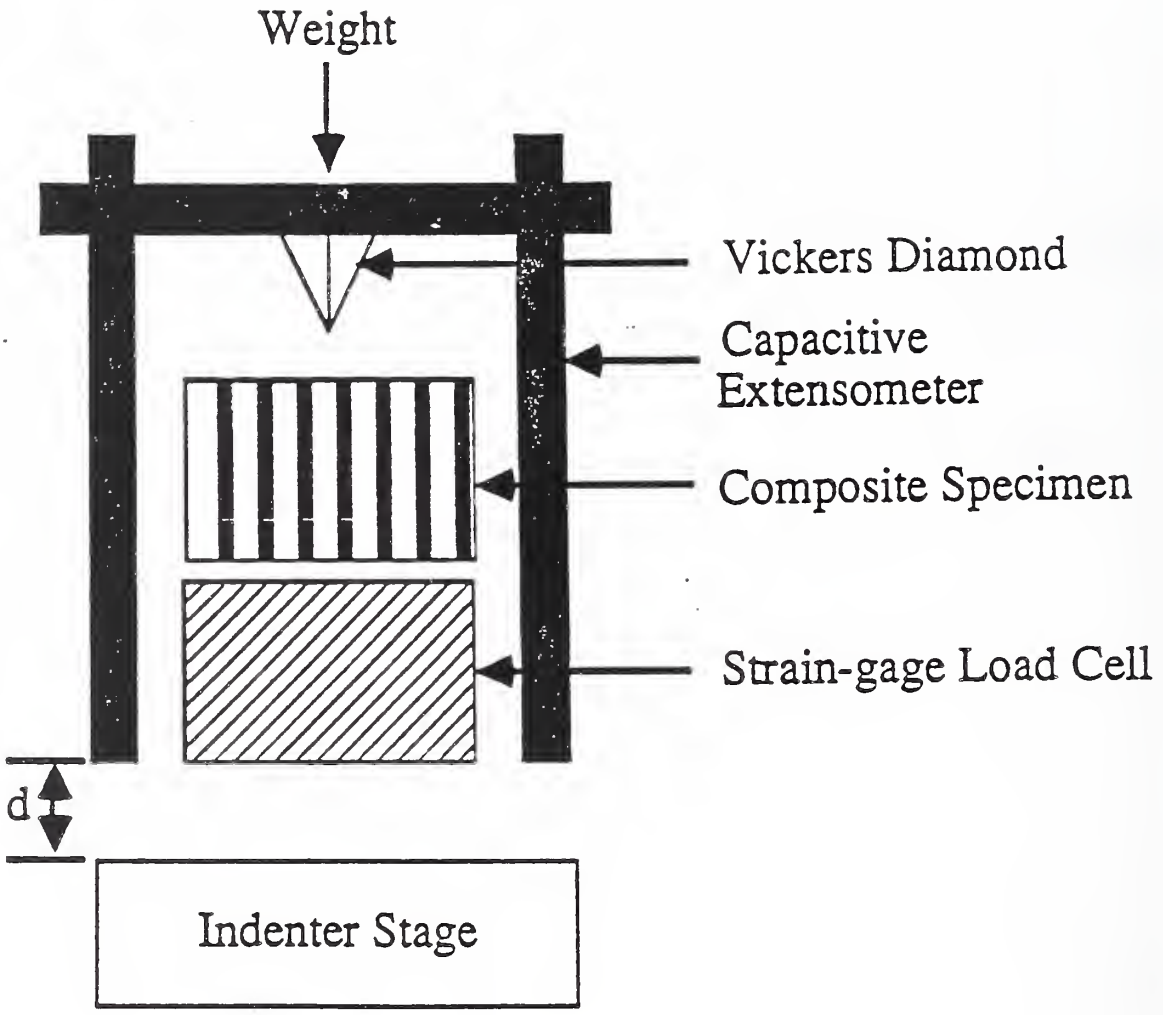
Weight
Vickers Diamond
Capacitive
Extensometer
Composite Specimen
Strain-gage Load Cell
d
Indenter Stage

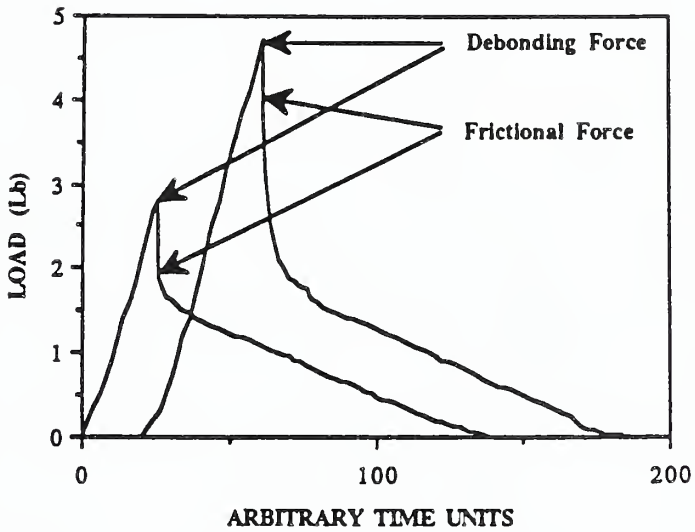
Debonding Force
Frictional Force
LOAD (Lb)
0
1
2
3
4
5
0
100
200
ARBITRARY TIME UNITS

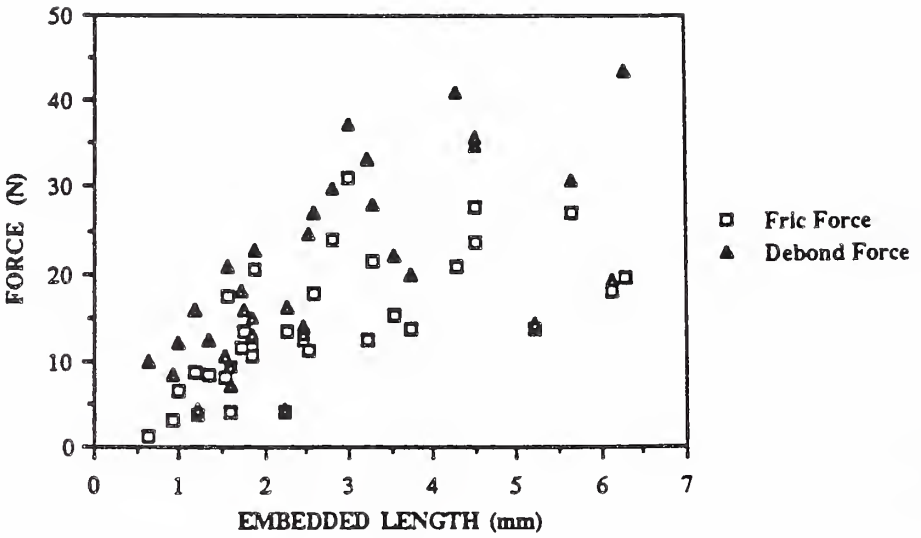
50
40
30
20
10
0
FORCE (N)
0
1
2
3
4
5
6
7
EMBEDDED LENGTH (mm)
Fric Force
Debond Force

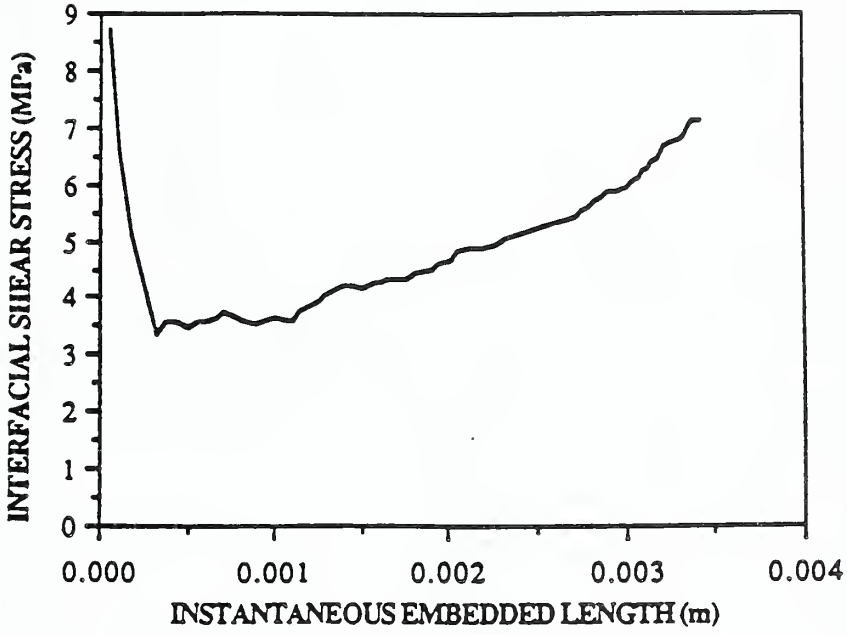
INTERFACIAL SHEAR STRESS (MPa)
9
8
7
6
5
4
3
2
1
0
0.000
0.001
0.002
0.003
0.004
INSTANTANEOUS EMBEDDED LENGTH (m)

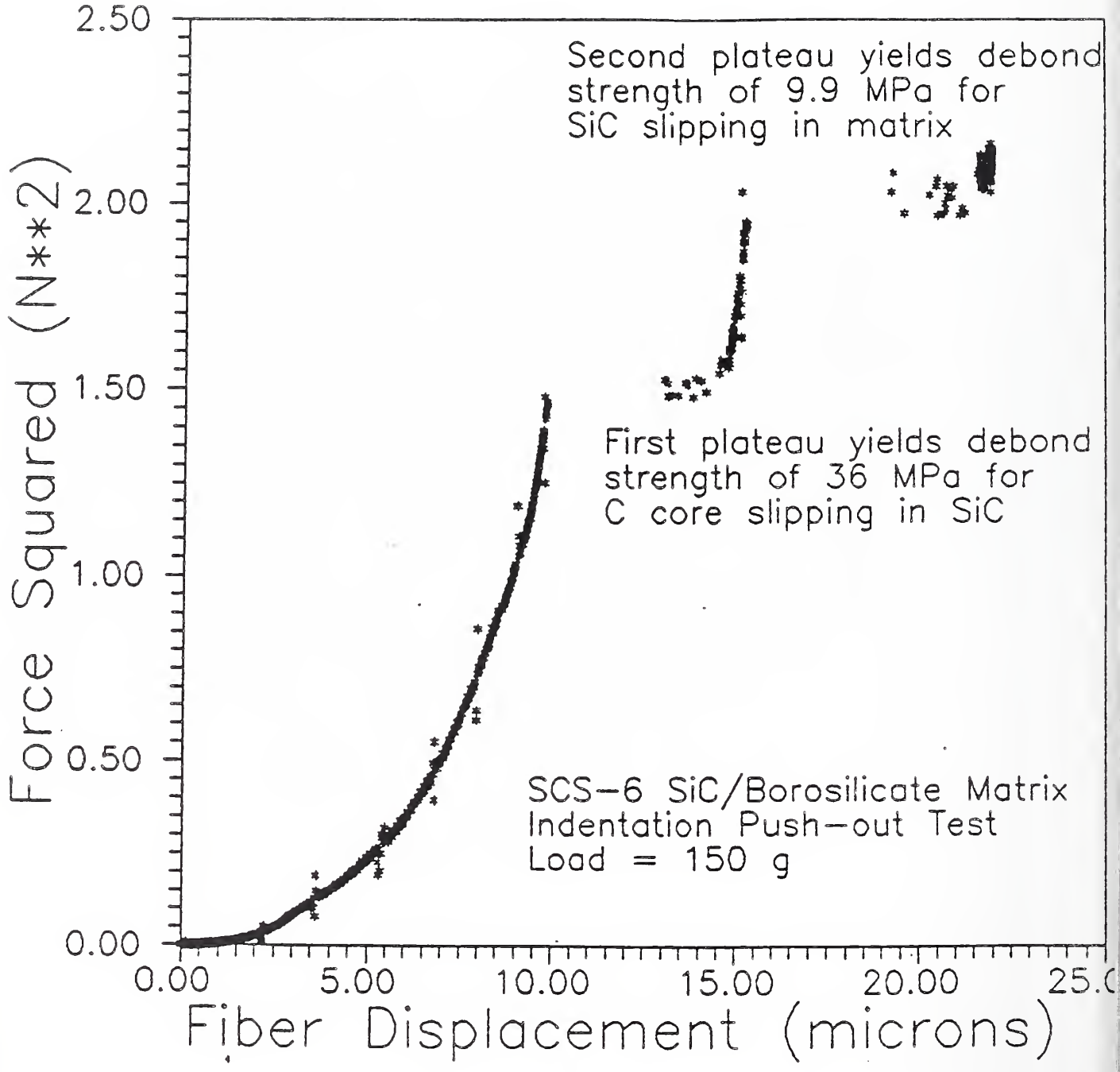
Second plateau yields debond strength of 9.9 MPa for SiC slipping in matrix
First plateau yields debond strength of 36 MPa for C core slipping in SiC
SCS-6 SiC/Borosilicate Matrix
Indentation Push-out Test
Load = 150 g
Force Squared (N**2)
2.50
2.00
1.50
1.00
0.50
0.00
0.00
5.00
10.00
15.00
20.00
Fiber Displacement (microns)

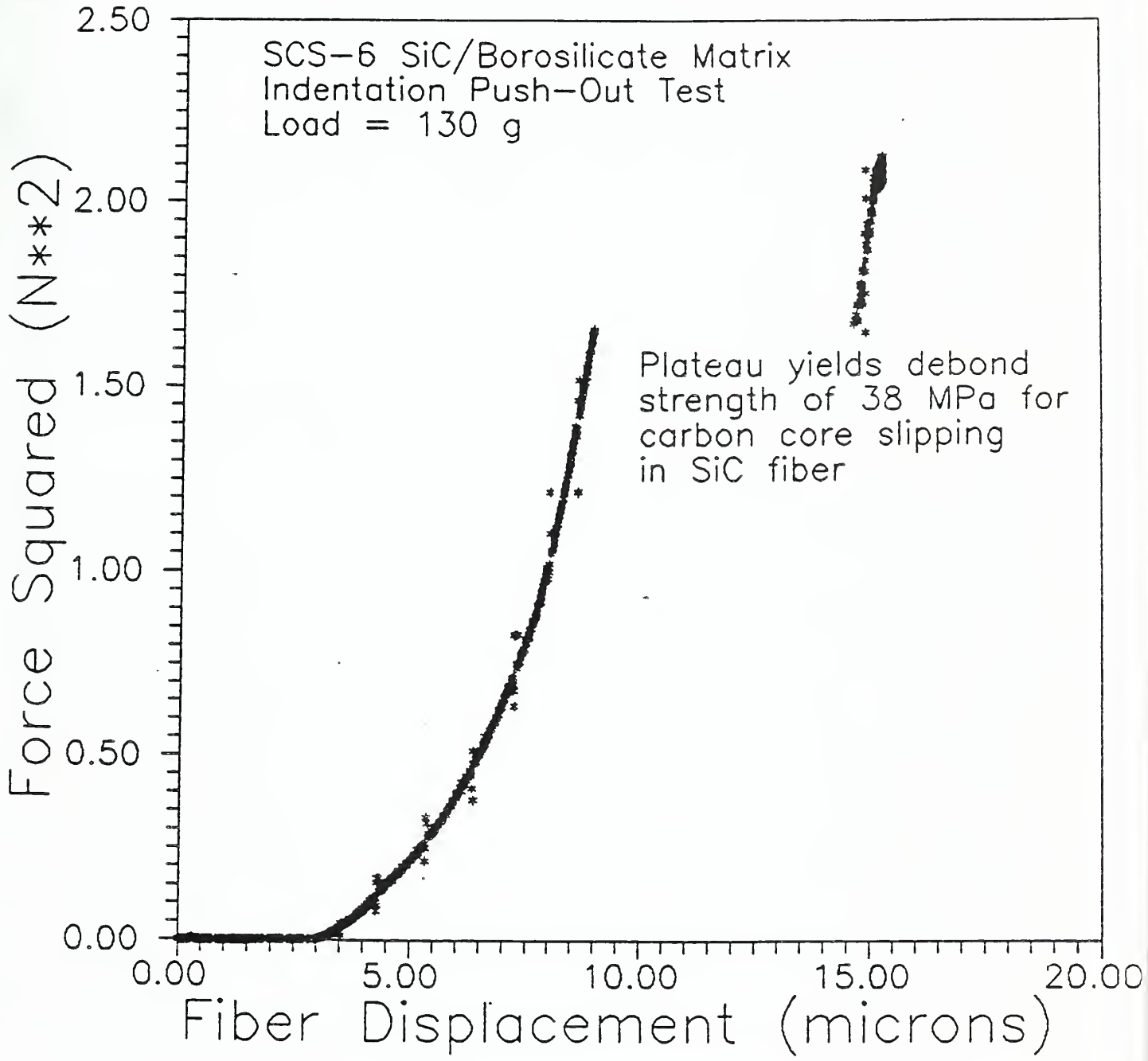
SCS–6 SiC/Borosilicate Matrix
Indentation Push–Out Test
Load = 130 g
Plateau yields debond strength of 38 MPa for carbon core slipping in SiC fiber
Force Squared (N**2)
2.50
2.00
1.50
1.00
0.50
0.00
0.00
5.00
10.00
15.00
20.00
Fiber Displacement (microns)

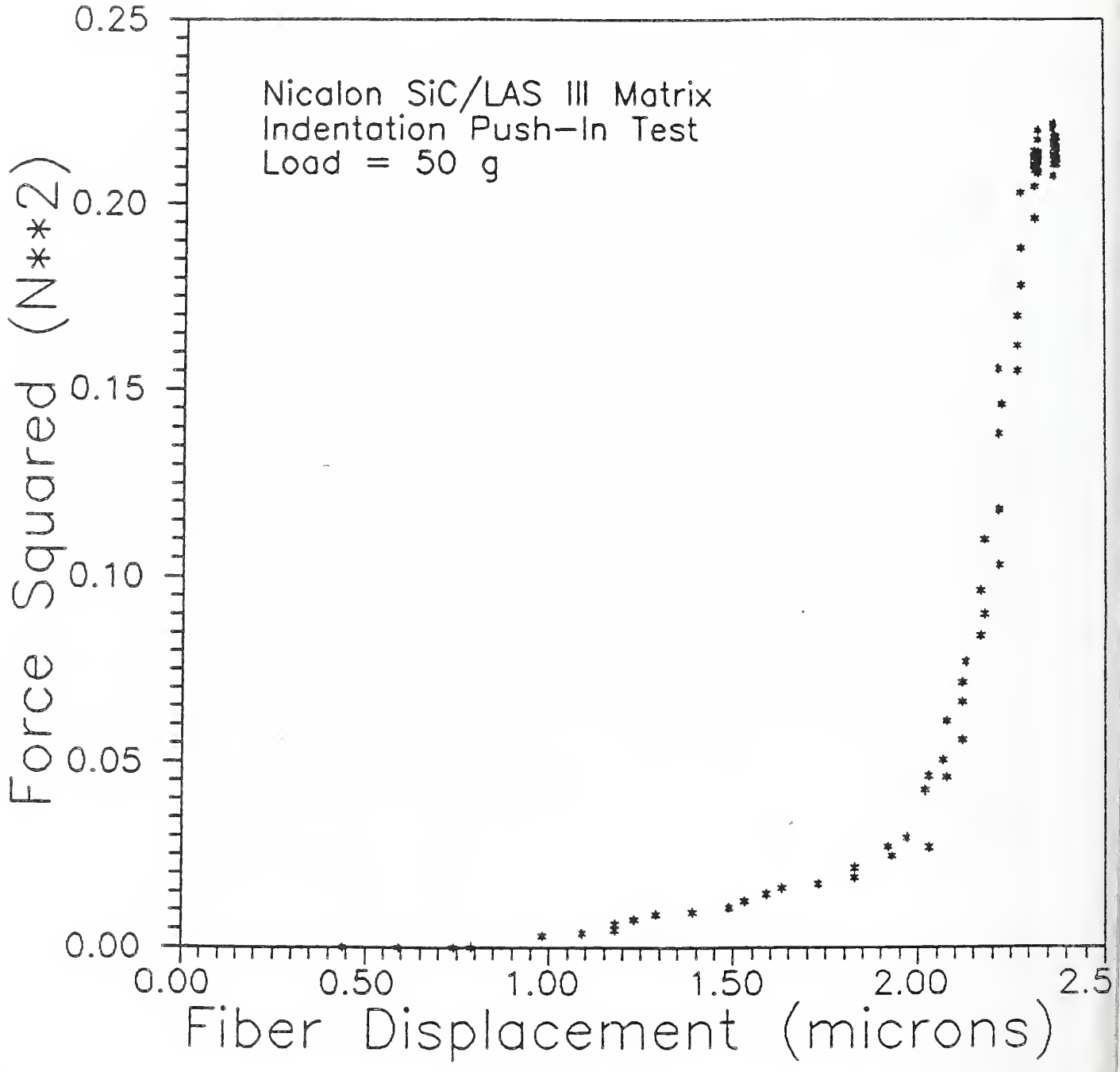
Nicalon SiC/LAS III Matrix
Indentation Push-In Test
Load = 50 g
Force Squared (N**2)
0.25
0.20
0.15
0.10
0.05
0.00
0.00
0.50
1.00
1.50
2.00
2.5
Fiber Displacement (microns)

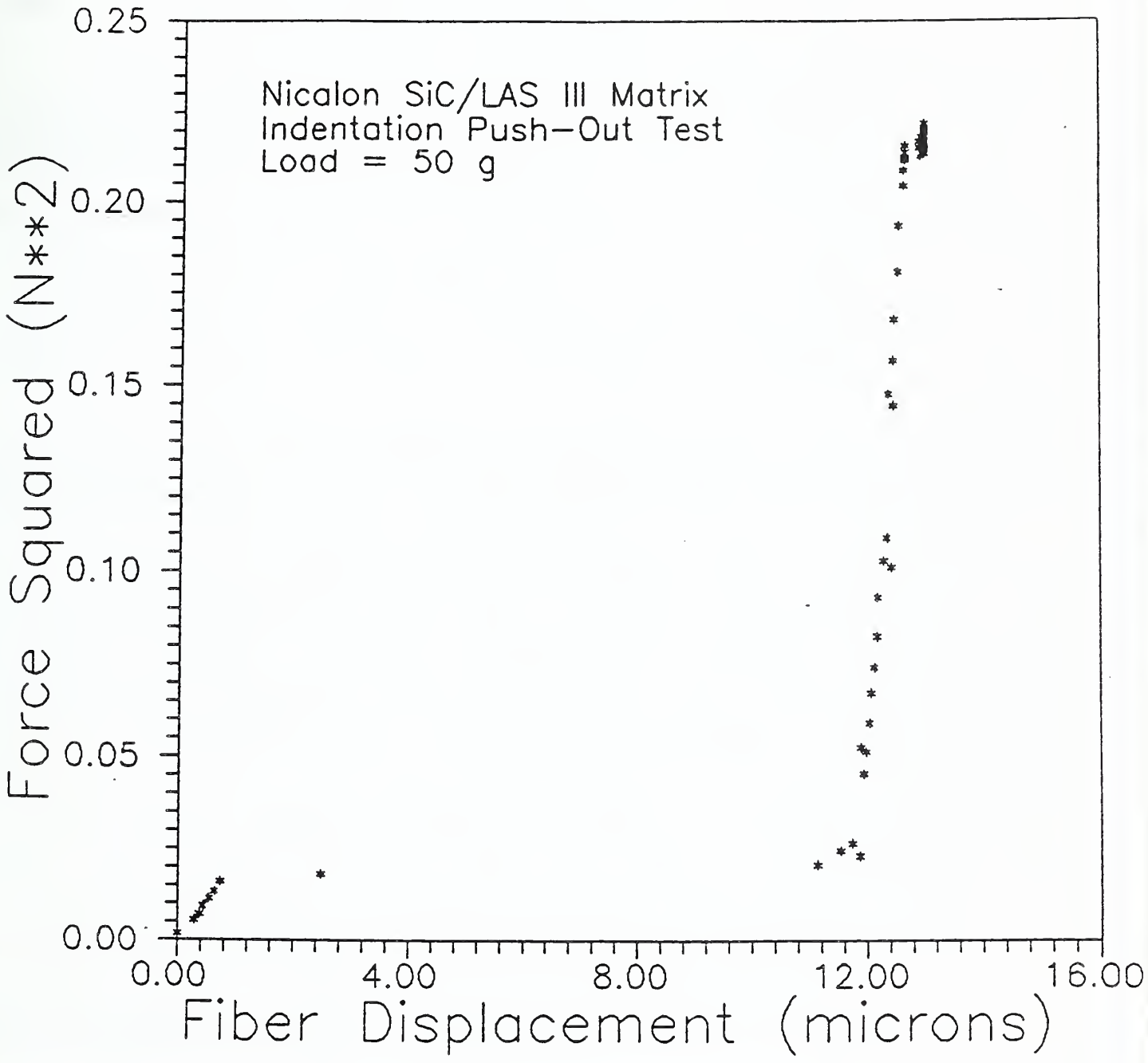
Nicalon SiC/LAS III Matrix
Indentation Push-Out Test
Load = 50 g
Force Squared (N**2)
0.25
0.20
0.15
0.10
0.05
0.00
0.00
4.00
8.00
12.00
16.00
Fiber Displacement (microns)

NIST-114A
(REV. 3-89)

U.S. DEPARTMENT OF COMMERCE
NATIONAL INSTITUTE OF STANDARDS AND TECHNOLOGY

BIBLIOGRAPHIC DATA SHEET

1. PUBLICATION OR REPORT NUMBER
NISTIR89-4079

2. PERFORMING ORGANIZATION REPORT NUMBER

3. PUBLICATION DATE

4. TITLE AND SUBTITLE

"Determination of Fiber/Matrix Interfacial Properties of Ceramic and Glass Matrix Composites".

5. AUTHOR(S)

David C. Cranmer

6. PERFORMING ORGANIZATION (IF JOINT OR OTHER THAN NIST, SEE INSTRUCTIONS)

U.S. DEPARTMENT OF COMMERCE
NATIONAL INSTITUTE OF STANDARDS AND TECHNOLOGY
GAITHERSBURG, MD 20899

7. CONTRACT/GRANT NUMBER
N00014-C-0096

8. TYPE OF REPORT AND PERIOD COVERED
Interim, 1/1/86 - 1/1/88

9. SPONSORING ORGANIZATION NAME AND COMPLETE ADDRESS (STREET, CITY, STATE, ZIP)

SDIO/IST
c/o Office of Naval Research, 800 N. Quincy Ave.
Arlington, VA

10. SUPPLEMENTARY NOTES

[ ] DOCUMENT DESCRIBES A COMPUTER PROGRAM; SF-185, FIPS SOFTWARE SUMMARY, IS ATTACHED.

11. ABSTRACT (A 200-WORD OR LESS FACTUAL SUMMARY OF MOST SIGNIFICANT INFORMATION. IF DOCUMENT INCLUDES A SIGNIFICANT BIBLIOGRAPHY OR LITERATURE SURVEY, MENTION IT HERE.)

The work described herein is primarily related to the development and use of several techniques for determining the fiber/matrix interfacial properties of ceramic and glass matrix composites. The specific techniques utilized are the double cleavage drilled compression (DCDC), indentation push-in, indentation push-out, and single fiber pull-out tests. The DCDC test provides direct experimental observation of the crack-fiber interactions, thus allowing us to more readily determine the effects of the fiber/matrix interface on the properties of the composites. The indentation techniques and the pull-out test provide information on the debond strength of the fibers from the matrix and interfacial frictional stress required to pull the fibers out of the matrix.

The emphasis has been on understanding what happens at the interface, and has focussed on several model systems including SiC monofilament reinforced glasses (borosilicate, soda-lime-silica), and SiC fiber reinforced glass-ceramic. Measurements have been made of the interface properties as well as on the increase in toughness as a crack approaches the reinforcing fibers. Some of the effects of interface chemistry on the properties have also been considered, both experimentally and as it might relate to processing of the composite. Much of the work is expected to continue with a future emphasis on the high temperature aspects of ceramic and glass matrix composites.

12. KEY WORDS (6 TO 12 ENTRIES; ALPHABETICAL ORDER; CAPITALIZE ONLY PROPER NAMES; AND SEPARATE KEY WORDS BY SEMICOLONS)

13. AVAILABILITY

[X] UNLIMITED

[ ] FOR OFFICIAL DISTRIBUTION. DO NOT RELEASE TO NATIONAL TECHNICAL INFORMATION SERVICE (NTIS).

[ ] ORDER FROM SUPERINTENDENT OF DOCUMENTS, U.S. GOVERNMENT PRINTING OFFICE, WASHINGTON, DC 20402.

[ ] ORDER FROM NATIONAL TECHNICAL INFORMATION SERVICE (NTIS), SPRINGFIELD, VA 22161.

14. NUMBER OF PRINTED PAGES
80

15. PRICE
A05

ELECTRONIC FORM